EXPERIMENTAL INVESTIGATION OF A MAGNETIC INDUCTION PEBBLE-BED HEATER WITH APPLICATION TO NUCLEAR THERMAL PROPULSION

by

ROBERT MICHAEL TALLEY

JOHN BAKER, COMMITTEE CHAIR
CLARK MIDKIFF
ROBERT TAYLOR

A THESIS

Submitted in partial fulfillment of the requirements
for the degree of Master of Science in the
Department of Mechanical Engineering
in the Graduate School of
The University of Alabama

TUSCALOOSA, ALABAMA

2014

ABSTRACT

NASA explored the idea of nuclear thermal rockets in the 1950's and 60's and has recently shown interest in reviving the nuclear rocket program in an attempt to reach manned mission to Mars by 2035. One problem with nuclear rockets is finding ways to test them inside the atmosphere. NASA's Stennis Space Center has considered using a non-nuclear device to simulate a nuclear reactor during testing. The reactor is responsible for heating the propellant to over 1,922 K (3,000 °F), so the reactor simulator should be capable of heating to this temperature. A pebble-bed heater at Glenn Research Center was used for nuclear rocket testing in the past; however, the device no longer exists. This particular pebble-bed heater used hot gases to heat the pebble bed made of high melting temperature ceramics and was able to reach 2,755 K (4,500 °F) but could only sustain the temperature for 30 seconds at most.

If the pebbles were heated by magnetic induction, then heat would consistently be generated within the heater, and tests could run longer. Magnetic induction heats a ferrous metal by inducing a current on its surface and by rapidly reversing a magnetic field surrounding the metal. Unfortunately, it was found that a magnetic induction pebble-bed heater using steel could not reach 1,922 K (3,000 °F) due to the Curie and melting temperatures. However, the device could be used if a higher melting temperature metal was found that was also magnetic.

A small-scale pebble-bed heater heated by magnetic induction was designed, built, and tested to analyze its behavior at 27 different combinations of flow rates, pebble sizes, and power levels. The temperature changes were recorded for each test. With this data, a relationship between dimensionless heat transfer, dimensionless power, and Reynolds number was found.

LIST OF ABBREVIATIONS AND SYMBOLS

A_{air}	Effective area of air in pipe cross section
A_{steel}	Effective area of steel in pipe cross section
B	Flux density
c_p	Specific heat at constant pressure
DMM	Digital Multimeter
DPT	Differential Pressure Transducer
g_o	Acceleration due to gravity
GRC	Glenn Research Center
H	Magnetizing Force
I	Current
I_{sp}	Specific Impulse
k_{air}	Thermal conductivity of air
$k_{plastic}$	Thermal conductivity of plastic
k_{steel}	Thermal conductivity of steel
L_{c_air}	Characteristic length of air in the pipe
L_{c_steel}	Characteristic length of carbon steel in the pipe
$\dot{m}$	Mass flow rate
m_{balls}	Mass of all balls inside the cylinder
MOSFET	Metal-Oxide Semiconductor Field-Effect Transistor
N_{HT}	Dimensionless Heat Transfer

N_P	Dimensionless Power
NASA	National Aeronautics and Space Administration
NERVA	Nuclear Engine for Rocket Vehicle Application
NPT	National Pipe Thread
NRS	Nuclear Reactor Simulator
NTP	Nuclear Thermal Propulsion
NTR	Nuclear Thermal Rocket
Q_{cond}	Power given to heat the pebbles by conduction
Q_{conv}	Power given to heat the air by convection
Q_{loss_wall}	Power lost due to heat leaving through the pipe wall
$Q_{remaining}$	Power not used for convection or escaping through the pipe wall
P	Power
PBH	Pebble-Bed Heater
R_{air}	Resistance of air
R_{steel}	Resistance of carbon steel
Re	Reynolds number
r_{in}	Inner pipe radius
r_{out}	Outer pipe radius
SA_{balls}	Surface area of all balls inside the chamber
SSC	Stennis Space Center
T	Force of thrust

U	Velocity of air
V	Voltage
$\dot{V}$	Volumetric Flow Rate
V_{pipe}	Volume of the inside of the pipe
V_{steel}	Volume of steel inside the pipe
ΔP	Change in pressure through the heating chamber
ΔT	Change in temperature through the heating chamber
δ	Skin depth
ω	Frequency of current
μ	Permeability of material
σ	Electrical conductivity of material
ρ	Density
ν	Kinematic viscosity

ACKNOWLEDGMENTS

I have several people to thank for assisting me in fulfilling my research and thesis. Most importantly, I would like to thank Dr. John Baker for his excellent guidance and wisdom over the last two years. Dr. Baker has been very helpful and always made time for me when I needed him. I would also like to thank Dr. Clark Midkiff and Dr. Robert Taylor for agreeing to be my committee members, for their input on my thesis paper, and for their assistance throughout my graduate program. Graduate school would not have been possible without the Graduate Teaching Assistantship granted to me by Dr. Keith Williams, Dr. Hwan Sic Yoon, and the Mechanical Engineering department.

I am extremely indebted to Mr. David Coote and Dr. Harry Ryan at NASA's Stennis Space Center for hiring me as an intern in the summer of 2012, training and educating me over my term, and providing me with valuable experience that assisted in the making of this thesis.

Ken Dunn and the men at The University of Alabama's machine shop were very generous about cutting and sweating some pipe pieces for me on short notice and machining other parts of the experiment. The University of Alabama's 3D Printing Lab also did a phenomenal job printing off one of the key components of the experiment. Every purchase I made had to go through Ms. Lisa Hinton, so I would like to thank her for her hard work as well. Ms. Betsy Singleton and Ms. Lynn Hamric were also a huge help throughout my graduate studies. Lastly, I would like to thank Mindy, my family, and my friends for supporting my decision to attend graduate school at The University of Alabama and being there for me along the way.

CONTENTS

LIST OF TABLES

LIST OF FIGURES

CHAPTER 1

INTRODUCTION

From 1955 to 1972 NASA explored the idea of nuclear thermal propulsion and nuclear thermal rockets with the NERVA (Nuclear Engine for Rocket Vehicle Application) program. NERVA was successful in building and testing a nuclear rocket engine, but the engine was never approved and used on a rocket in outer space. In 1972 the program was cancelled due to lack of funding.

Recently, NASA has been interested in reviving the idea of nuclear thermal rockets (NTR). Nuclear rockets provide double the specific impulse (I_{sp}) compared to that of current chemical rockets and would therefore make manned exploration to Mars possible by significantly reducing the round trip time [2]. One major obstacle of the nuclear thermal rocket revival effort that did not exist in the 1950's and 60's is testing the nuclear engines in the earth's atmosphere. Several solutions for testing the engines were proposed at NASA's Stennis Space Center (SSC). One of the solutions being to find a nuclear reactor simulator (NRS) that was non-nuclear but could still heat the hydrogen rocket propellant to the same temperature that the nuclear reactor would, which was between 1,922 K and 3,033 K (3,000 °F and 5,000 °F). The most promising simulator was a pebble-bed heater (PBH) [48,58,59]. NASA currently has at least two pebble-bed heaters—one at Glenn Research Center and one at Stennis Space Center [25,34,43].

In order to simulate a nuclear reactor, the pebble-bed heater would first need to heat a large number of small steel or ceramic spheres in an internal chamber and raise their temperature to over 1,922 K (3,000 °F) before running the hydrogen propellant through the pebble bed. The hydrogen would heat up as it passed over the spheres and then make its way to the rocket engine

interface. This would allow the engineers to test their rocket engine under nuclear conditions and hopefully produce a working product without ever using nuclear materials.

Current pebble-bed heaters at NASA facilities use convection and hot gases to heat the spheres inside the pebble-bed heating chamber and have been known to reach temperatures up to 2,755 K (4,500 °F). However, this convection method only allows for a limited testing window as the spheres will quickly cool off as the heat is taken away from them, and the hydrogen will no longer exit at the desired temperature. This will result in a very short test time for an engine that would normally be used for at least several minutes.

The purpose of this research was twofold. The first reason being to determine if magnetic induction could be used instead of hot gases when heating the spheres inside the pebble-bed heater. This would achieve longer run times at a consistent high temperature during nuclear engine testing. Secondly, a dimensionless analysis would be performed in order to predict the outcome of future pebble-bed heaters. Therefore, the research also included an experiment that demonstrates the capabilities of a small-scale magnetic induction pebble-bed heater and the effects of certain variables on the system. A small-scale pebble-bed heater and an induction heater were designed, constructed, and tested in order to analyze the system's behavior. The experiment was built so that the variables could be easily monitored and varied. The pebble-bed heater was tested at a series of flow rates, power levels, and pebble sizes.

CHAPTER 2

BACKGROUND AND LITERATURE REVIEW

A) Nuclear Thermal Propulsion

NASA has a stated goal of sending humans beyond the moon by 2025 and sending humans on a roundtrip mission to Mars by 2035 [5]. With its increased thrust-to-weight ratio and higher specific impulse, the best option for manned missions beyond the moon is nuclear thermal propulsion [2].

When considering which engine to put on a rocket, one characteristic that is of utmost importance is specific impulse. Specific impulse (I_{sp}) in a rocket engine is the ratio of thrust to propellant mass flow rate as seen in equation 1 [2]. Higher I_{sp} is more desirable because the engine is producing more thrust and going farther for every kilogram of fuel. Therefore, an engine with a higher specific impulse is more efficient. In this sense, specific impulse is very similar to miles per gallon on a car. Current chemical rockets combust liquid hydrogen and liquid oxygen to generate thrust out the nozzle, and the best chemical rockets can only achieve 450 seconds of specific impulse [2]. Newer methods of powering rockets, such as nuclear fission, are able to get much higher I_{sp}. Current nuclear technology with the use of hydrogen propellant can achieve between 800 and 900 seconds of specific impulse, double that of a chemical rocket [3]. Although, research has been done into propellants for nuclear propulsion that can produce even higher specific impulse. The fuels are still in the process of being tested but could be ready before 2035 [2].

$$I_{sp}[s] = \frac{T\,[N]}{\dot{m}\left[\frac{kg}{s}\right]} * \frac{1}{g_o\left[\frac{m}{s^2}\right]} \qquad \text{Eq. 1}$$

In the 1950's and 60's several companies and agencies discovered these specific impulse benefits and experimented with nuclear thermal propulsion (NTP), but no agency at that time

succeeded in producing a space-ready, approved engine and eventually lost funding. One of the most successful nuclear programs was NERVA (Nuclear Engine for Rocket Vehicle Application), which was headed by NASA and the US Atomic Energy Commission [45]. The NERVA team was able to build and test a nuclear rocket engine as seen in figures 1 and 2.

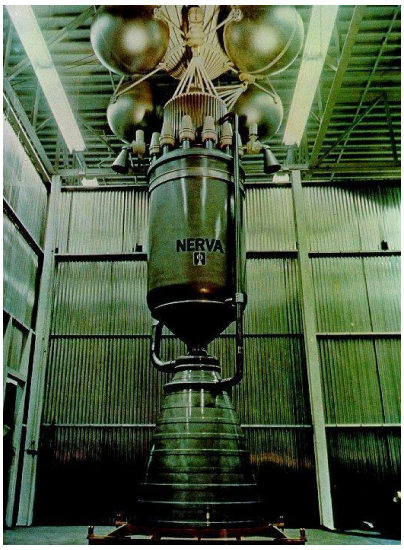

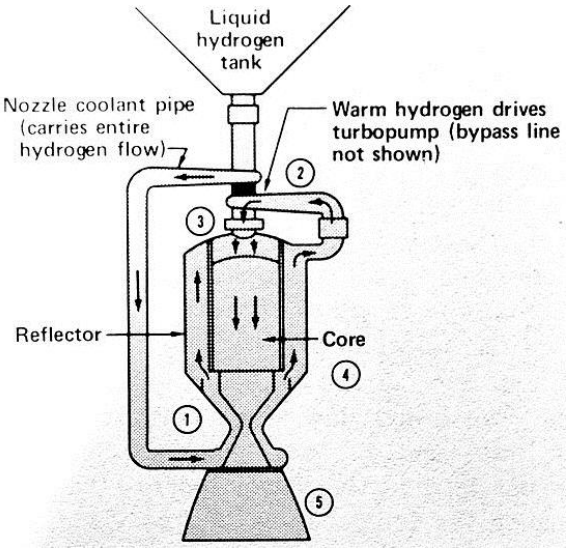

Figures 1 and 2. NERVA nuclear fission rocket engine and schematic.

Credit: NASA (Public Domain) [7,36].

NERVA's engine was a nuclear fission, solid-core, flight-rated, graphite engine designed to provide 333 kN (74,861 lb) of thrust with an I_{sp} of 825 seconds, and weighing 92.5 kN (20,800 lb) [55]. The NERVA engine had a ten-hour supply of fuel and could power up and down as many as 60 times allowing it to conserve fuel when thrust was not needed [55]. It consisted of three main sections: the turbopumps, the nuclear reactor, and the nozzle (Figure 3); however, this discussion will focus mainly on the reactor [36]. The hydrogen would start in the storage tank, make its way down to cool the nozzle, proceed to the turbopumps, run through the nuclear fission reactor, and blast out of the nozzle, generating thrust [55]. Despite its apparent success, there were problems with the overall design and especially the reactor [21]. Several of the main

issues with the reactor were caused by high operating temperatures in a corrosive atmosphere as well as drastic temperature variations across the reactor [21]. This caused several reactors to fail in the testing process. These problems, in addition to others, led to the downfall of the project, and in 1972 the NERVA engine was decommissioned.

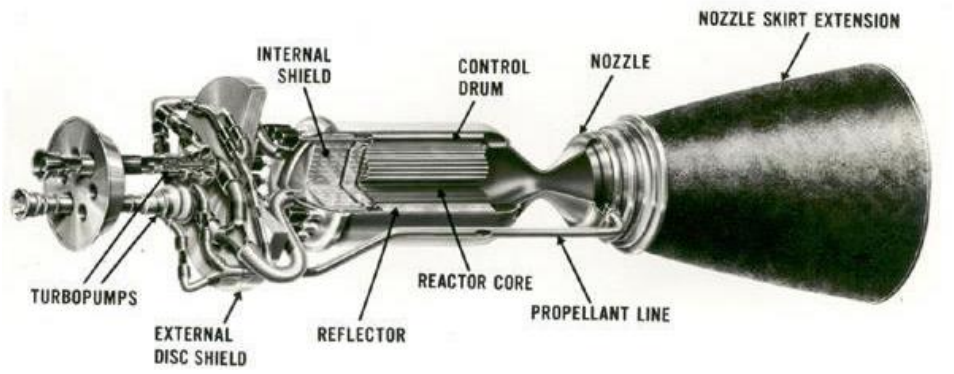

Figure 3. Cut away of NERVA engine. Credit: NASA (Public Domain). [36].

There was another promising program at the same time as NERVA called Project Rover which existed from 1955 to 1973. The Rover team was able to run 22 full power tests for a total duration of 109 minutes [30]. The engine operated at a thrust of 929,678 N (209,000 lb) and a specific impulse just over 900 seconds with the hydrogen propellant heated to 2,533 K (4,100 °F) [30]. As successful as Rover was, it was forced to shut down due to the insufficient technology of the time and lack of funding, as was the case with NERVA. Since its closing, the facilities have been torn down, so very little of Project Rover remains. After NERVA and Rover's decommission, several companies and programs have tried to bring back the nuclear rocket engine program using similar technology, but none have succeeded.

Once more, NASA is attempting to develop a nuclear rocket engine in order to meet the benchmark of sending a man on a roundtrip mission to Mars by 2035. NASA has asked their Stennis Space Center engine testing facility (Figures 4 and 5) to run and analyze the nuclear

rocket engine on their test stands after the engine has been constructed [48,58,59]. The engineers at NASA are studying the pros and cons of the NERVA and Rover programs, so that they can recreate and improve the nuclear engine. However, the testing process will prove to be a major setback because the world is much more environmentally and safety conscious than it was in the 1950's and 60's. The hurdles that now have to be tackled include containing nuclear radiation, residual radioactivity, worker safety, environmental contamination, and nuclear security concerns [55].

Figures 4 and 5. Engine test stands at Stennis. Credit: NASA (Public Domain) [42,46]

In a normal flight, the nuclear reactor is responsible for raising the temperature and pressure of the hydrogen, which will then propel the rocket. During the testing process, a nuclear reactor simulator (NRS) will be used to accomplish the same task in order to avoid all nuclear aspects, which will then eliminate radiation poisoning, contamination, and all the other negative effects to the environment and workers [48,58,59]. Several possible simulator devices include a hydrogen boiler, a plasma arc heater, and a pebble-bed heater. After a several month-long study, NASA Stennis decided that the pebble-bed heater would be the best option. The pebble-bed

heater (PBH) was chosen because it is capable of reaching high temperatures and pressures and can be easily controlled to reach a more specific temperature.

In order to safely and efficiently test a nuclear thermal rocket engine, the parameters listed below must be met by the pebble-bed heater at the interface with the engine's nozzle [58]. The exact temperature, pressure, and flow rate will depend on the specific engine.

- Fluid interface temperature = 1,922 – 3,033 K (3,000 – 5,000 °F)
- Fluid interface pressure = 2,068,427 – 6,894,757 Pa (300 – 1000 psig)
- Fluid mass flow rate = 22.68 – 68.04 kg/s (50 – 150 lb_m/s)

B) Pebble-Bed Heaters

A pebble-bed heater is a large cylinder with an internal chamber, which contains a large number of steel or ceramic spheres called the "pebble bed" or "pebble matrix." A pebble-bed heater should not be confused with a pebble-bed reactor. While the two are similar, the focus of the testing for NASA Stennis would involve a pebble-bed heater to avoid the nuclear aspects associated with a pebble-bed reactor.

A majority of pebble-bed heaters use convection in order to raise the temperature of the pebble matrix and subsequently the gas or liquid run through the pebbles, as seen in figure 6. Several more advanced models will even incorporate an elevator system to transport the pebbles from the bottom to the top in order to get a more even temperature distribution [76]. The first part of the heating process is to run nitrogen, air, or some less expensive gas with a high convection heat transfer coefficient into the pebble-bed heater [25]. Then, the gas is passed through electric heaters or burners in order to raise the temperature of the gas [25]. The gas

enters at ambient temperature and can then be heated all at once or in stages to just above the desired overall temperature. Next, the hot gas flows through the pebble matrix for 5 to 24 hours, depending on the size of the pebble-bed heater, so that the temperature of each sphere inside the chamber is uniform throughout the matrix at the end of the time period [25]. Once the temperature is uniform, the first gas ("Gas 1") is shut off.

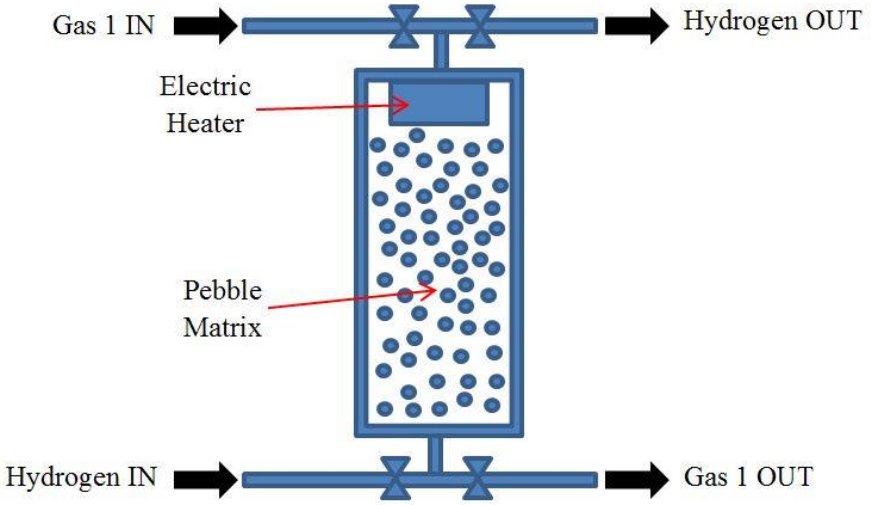

Figure 6. Schematic of a convection-heated pebble-bed heater.

Immediately after switching off the first gas, the hydrogen is pumped into the pebble-bed heater [25]. The hydrogen flows through the hot pebble matrix in the opposite direction as the previous gas and exits the heater. The exit temperature is initially at the desired temperature for the engine interface but will slowly decrease in temperature as the test goes on and the spheres cool off, so the tests should not exceed 30 seconds with this method [63].

NASA currently has at least two pebble-bed heaters: one at Glenn Research Center (GRC) and one at Stennis Space Center (SSC) [25,34,43]. The pebble-bed heater at Glenn Research Center was located in their wind tunnel and used high melting temperature ceramics instead of steel in the pebble matrix to allow for higher temperatures, since steel would melt at

any temperature above 1,811 K (2,800 °F) [43]. This wind tunnel facility was originally constructed in 1966 as the Hydrogen Heat Transfer Facility for the NERVA program and the development of nuclear rocket engines [43]. The pebble-bed heater was capable of heating hydrogen to 2,755 K (4,500 °F), until the heater was converted in 1969 to a 3 megawatt graphite core heater, and the building became the Hypersonic Tunnel Facility [43]. The new facility used the modified pebble-bed heater to heat gaseous nitrogen and then mix it with pure, clean gaseous oxygen to produce a very accurate air representation. Even though Glenn Research Center has permanently transformed their pebble-bed heater, they have still demonstrated that it is possible for a pebble-bed heater to reach such high temperatures. There could also be old nuclear engine test data from the 1960's that would help today's engineers produce an even more suitable pebble-bed heater than Glenn Research Center had created before.

Stennis Space Center's pebble-bed heater is a bit smaller in size and not as powerful compared to Glenn Research Center's. It has only been tested up to 978 K (1,300 °F) at 34,473,786 Pa (5,000 psia) and is therefore insufficient for nuclear thermal engine testing [63]. The pebble-bed heater at Stennis currently uses steel spheres with melting temperatures around 1,366 K (2,000 °F) and therefore would need to be modified for testing at higher temperatures.

If Stennis could upgrade their pebble-bed heater to the same style and specifications as Glenn Research Center's heater before the modification or build an entirely new one based off of GRC's, then the heater would be capable of achieving the same 2,755 K (4,500 °F) as before. This temperature is suitable for nuclear testing and would therefore make the pebble-bed heater an appropriate nuclear reactor simulator. However, even after the pebble-bed heater modification, the facility would still only be able to run approximately a 30 second test at these

high temperatures before the temperature of the spheres would begin to drastically fall off at a rate close to 7.22 K/s (13 °F/s) [63].

In order to resolve the issue of the short run time, this study has been conducted to experiment with a pebble-bed heater that has its pebble matrix heated by magnetic induction instead of hot gases. The new design will be analyzed to see if it will be capable of reaching the temperatures necessary to make it an acceptable nuclear reactor simulator. Due to the nature of magnetic induction, the new method would allow tests to be run for extended periods of time at a consistent high temperature.

C) Magnetic Induction Heating

Induction heating is a non-contact, flameless process of heating a ferrous metal by inducing a large current on its surface, while it is inside a constantly changing electromagnetic field [75]. Michael Faraday first discovered this concept in 1831. He noticed that electric current is generated in a metal by the fluctuation of a high frequency current in another metal directly next to it [41]. This generated current produces heat in the metal [41]. It was later found that heat loss through electromagnetic induction could be transformed into productive heat energy by using it as an electric heating system, which became known as an induction heater.

The process of induction heating is highly effective, because the heat is generated without any flame by simply inducing an electrical current on the part [26]. It was found that the amount of heat generated could be increased if the fluctuating high frequency current was also used to rapidly change a magnetic field which would create more heat due to friction at the molecular level [53]. Therefore, the induction heater took on the shape of a coil, so that it could both induce

a current and create an alternating magnetic field by putting the piece to be heated inside or near the coil.

General benefits to all induction heaters include less power consumed, high efficiency, no moving parts, and quick response time [26]. Induction heaters can consume as little as 10 watts but still heat an object to several hundred Kelvin. Naturally, the heater is capable of greater temperatures at higher power levels. Induction heaters have contributed to society over the past century as engineers began to find uses for the technology including heating, melting, hardening, welding, and forging [75]. It was even used by the US military in World War II for hardening engine parts [26]. The technology is most commonly found today in the kitchen and in pipe welding equipment [1,60].

By using induction heated stoves and other cooking appliances, fewer burns are possible in the kitchen, and therefore they are safer for everyone, especially houses with children. Since magnetic induction only heats ferrous metal, someone can place their hand on the stove top with the stove turned on and not be harmed or feel any heat [1]. Induction stoves are also highly efficient and heat quickly, allowing the consumer to save money and time [1,38]. The design of the induction stove is quite simple as well; the system is comprised of the cooking surface on top, the concentric spiral-wound coil in the middle, and a magnetic substrate below [38]. A pot with a ferrous metal bottom is merely placed on top of the stove and within a minute or two the pot can reach boiling temperature. Thanks to all the benefits it provides, induction stoves have become quite common in households around the United States.

Over the past few decades, it has become more widely acceptable to use magnetic induction to weld either pipes or metal tubing together at the seam during production. After the metal is curled into a circular cylinder, current flows from one sliding contact along the first side

of a moving open pipe to the top of the pipe where the edges meet, and then the current flows down the other side to a second sliding contact [31]. This produces a large induced current and focuses all of the heat at the seam as the two edges are pressed together by rollers, solidifying the weld [31]. Pipes and tubes can be welded at hundreds of meters per minute using this method, proving that induction heaters are helpful and useful technology in this field.

An induction heater typically consists of several main parts: a power supply to deliver high voltage and current, a copper or brass work coil to carry the current, and transistors to rapidly alternate the flow direction of the current [61]. Induction heaters can be made in a variety of ways to perform a specific function. They can be customized by altering the circuitry and the work coil's shape for different strength levels, target areas, and work pieces to be heated. Simple circuits exist for low temperature induction heating below 533 K (500 °F); but if a higher temperature is desired, then a more intricate circuit must be used. The work coil may be wound several ways: a single loop, a multiple loop center-tapped solenoid, a multiple loop concentric spiral, or several less popular designs [35,60]. The way in which the coil is wound affects the size and shape of the area being heated. A single loop is better for localized heating over a small area. The multi-loop center-tapped solenoid design is good if a larger area needs to be affected. The concentric spiral work coil is best for heating metal that is completely on one side of the coil, which is why it is used on pots for induction cooking [38]. For this study, the focus will be on the multiple loop center-tapped solenoid work coil in order to have a prolonged heating effect and heat up more of the steel spheres, see figure 7.

Figure 7. Multiple loop center-tapped solenoid work coil.

The induction heating process is the product of two simultaneous mechanisms: the skin effect and hysteresis loss [32]. For the heater to work, a source of high frequency electricity must send an alternating current through a solenoid coil of wire. This current will generate a strong magnetic field inside the coil. The strength of the magnetic field generated also increases as you increase the number of loops per unit length of the solenoid [64]. Any ferromagnetic metal object, termed "ferrous," introduced in or around the coil will cause a change in the existing magnetic field [22,37]. A current is subsequently generated on the surface of the ferrous object called an "induced current" or "eddy current" [53]. Eddy currents will be stronger on the inside of the coil compared to the outside, and the eddy current will be greater the closer the ferrous metal is to the coil [79]. This generated current has an inverse directional relationship with the current going through the coil and will flow in the opposite direction as depicted in figure 8 [6,60]. The induced current remains at the surface or "skin" of the object. This large current on the metal's surface in combination with the resistance of the ferrous object produces a substantial amount of heat and is referred to as the skin effect [6].

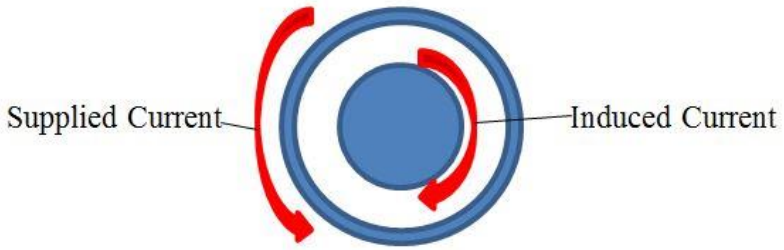

Figure 8. Induced current flowing in the opposite direction as the supplied current.

The quantity of heat generated is dependent on and proportional to the strength and intensity of the magnetic field as well as the frequency of the supplied current. The skin effect generates more heat than the hysteresis loss, so most of the heating occurs near the surface. It is beneficial to have most the heating occur near the surface in the case of the pebble-bed heater, since the induction heater will be used to heat the gas/liquid via convection as it flows over the spheres. To find out how deep the bulk of heating is taking place, the skin depth can be calculated using equation 2. The skin depth is the thickness from the outer wall to the depth where 86% of the total heat generation occurs from eddy currents [60,75]. If the ratio of the work piece's diameter to the reference depth is less than 4, then the process will not be very efficient [60].

$$\delta = \sqrt{\frac{2}{\omega\mu\sigma}} \qquad \text{Eq. 2}$$

where,

δ = skin depth

ω = frequency

μ = permeability of the material

σ = electrical conductivity of the material.

Hysteresis loss is the second heating mechanism associated with magnetic induction [67]. With the rapidly alternating direction of the driving current through the solenoid comes a rapidly alternating magnetic field. This causes the ion crystals inside the ferrous metal to repeatedly magnetize, demagnetize, flip to align with the new polarity, and magnetize again [60]. Every time the crystals flip, there is a large amount of heat produced inside the metal due to the friction between the molecules [67]. The amount of heat produced is not quite as high as the heat generated from the skin effect, but it still makes a sizable difference. Depicted in figure 9, a hysteresis loop is a plot showing the trace of the magnetic flux of the material (B) compared to the magnetizing force being applied to it (H) [47]. As the magnetic field is reversed, the trace will go from one extreme to another in a counter-clockwise rotation. A metal with a larger area inside the hysteresis loop will generate more heat [6].

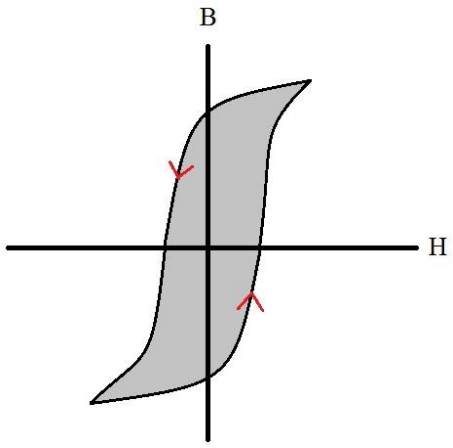

Figure 9. Hysteresis loop.

Unfortunately, while the magnetic permeability of ferrous materials is high at ambient temperature, there is a temperature called the Curie temperature where steels lose their magnetic properties [37]. For most grades of steel the Curie temperature is around 1,033 K (1,400 °F) [3,6]. Therefore heating above 1,033 K (1,400 °F) with an induction heater is possible, but it is

more difficult, since it must be accomplished with the skin effect alone after this point. To accomplish this, the amount of current supplied and consequently induced would have to be drastically increased once the steel reaches the Curie temperature to make any difference.

Evidence has been found of at least two previous magnetic induction pebble-bed heaters, proving that it can be done. Both devices were even similar in size to the one built in this experiment [9,78]. The first was built by a group in 2011 using a 200 kilowatt induction heater to heat three centimeter diameter pebbles, which would in turn heat the salt surrounding the pebbles [78]. The salt would function as a coolant to take away some of the heat [78]. It was being used to simulate the cooling process of the pebble core region of the high-temperature pebble-bed reactor at The University of California. The induction heater in their experiment was much more powerful than the heater built for this study. There were no results published in the report describing numerically or graphically the temperature to which the heater was able to achieve, and no dimensionless analysis was performed.

The second magnetic induction pebble-bed heater was mentioned in a 2011 report by a different group from the Science and Technology Facilities Council [9]. The researchers were testing the cooling rate of a solid target versus one that has a packed pebble bed on the inside [9]. The targets would be heated by induction and then cooled by flowing air/helium through the packed bed or around the solid target. They were successful in proving that a packed bed object would cool faster than a solid target of the same size, since the air could affect more of the surface area [9]. The report included several computational models of the air flow and temperature throughout the heated objects but still no dimensionless analysis.

While both of these reports dealt with a magnetic induction pebble-bed heater, neither demonstrated how the temperature would be affected under different conditions or the relationship between various dimensionless numbers.

CHAPTER 3

EXPERIMENT APPROACH

A) Designing the Pebble-Bed Heater

In February 2013, the idea to use a magnetic induction pebble-bed heater for the nuclear rocket program was first considered. The idea was that the metal spheres in the pebble matrix could be heated using electromagnetics instead of hot gases. To test this theory, research would have to be done on the limitations of this method, and a pebble-bed heater would have to be built and experimented on. A full-size pebble-bed heater can be anywhere from 3 to 7 meters (10 to 20 feet) tall, so it was deemed more practical with respect to cost, time, and space to design a small-scale pebble-bed heater. The device would be half a meter tall with the heating chamber being 15.24 cm (6") long.

Since the device would not be very tall, and the capabilities of the induction heater were unknown at the time, it was decided that the pebble holding chamber should not be very wide. The idea of a 5.08 cm (2") diameter was thrown around and strongly considered, but in the end a 2.54 cm (1") diameter pipe was determined to be more suitable to allow the magnetic field density to be twice as large so as to achieve higher temperatures.

The chamber material had to be non-ferrous, so that the induction heater coil, which would be wrapped around it, would only affect the pebbles inside and not waste heat on the chamber. After some research, several common materials were found to be non-ferrous that could work for this experiment including aluminum, brass, and copper [15]. Copper and brass were chosen over aluminum, since they were stronger than aluminum. Copper won out because while a majority of brass does not contain iron, there are several versions of brass which contain slight traces of iron and therefore would be affected by the induction heater if the wrong version

was purchased [65]. Even though copper was the most expensive and heaviest of the three, it would prove to be the most suitable choice initially. Once the diameter, length, and material had been determined, the 2.54 cm (1”) copper pipe for the experiment, pictured in figure 10, could be purchased from www.plumingsupply.com [56].

Figure 10. 2.54 cm (1”) diameter, rigid, type L, copper pipe.

In addition to the central pebble chamber, the device would need a way to measure the temperature and pressure both before and after the heat was applied in order to calculate the difference. Therefore, copper disk spacers would need to be inserted above and below the pebble matrix pipe segment. The spacers would need a way to attach to the central chamber, so the copper pipe now required a copper flange on either end as shown in figure 11. The flanges should have several holes for bolts to pass through, which would eventually secure the spacers to the flange. The spacers were designed so that fittings for a differential pressure transducer’s tube and a thermocouple probe could be screwed into the outside wall of each spacer without any air leaks. This would mean that the on-campus machine shop would have to drill out the holes and grooves in the curved side wall necessary for these two fittings. In addition to the holes for the fittings, the machine shop would also need to cut out the 2.54 cm (1”) diameter hole in the center for the fluid to flow through and the multiple holes for the bolts to pass through the spacer. The

copper disks should have the same diameter as the flanges and be 2.54 cm (1”) thick to allow enough space to make the holes in the side wall and have a little extra room left over. The copper flanges would come from Grainger, and the copper material for the spacers was taken care of by the machine shop [27]. The flanges that were purchased were 10.8 cm (4.25”) in diameter with four 1.588 cm (5/8”) holes equally spaced 90° apart for the bolts. The copper from the machine shop was 10.16 cm (4”) in diameter, since 10.8 cm (4.25”) could not be found.

Figure 11. Copper flange-pipe-flange assembly.

For the design of the pebble-bed heater experiment, it was determined that it would be best to do the test trials using only gas so as to avoid any possible electrical shock or shorts from a spilled or leaking liquid. Pebble-bed heaters are perfectly capable of heating and containing liquids; this was merely a precaution to avoid major setbacks. Air was chosen as the medium that was to be heated, since it has consistent properties, is free, and is readily available.

In the lab there was an air pump (Figure 12), which could supply up to 20 liters per minute of air (LPM) and had the fittings to connect to 0.635 cm (1/4”) tubing, making it an excellent candidate for the experiment. Therefore, 0.635 cm (1/4”) outer diameter was the size

for all air tubing to and from the pebble-bed heater. Conveniently, the lab also already had 0.635 cm (1/4”) low-density polyethylene clear tubing, which worked perfectly for the experiment because of its size, flexibility, and ability to withstand the hot air exiting the pebble-bed heater.

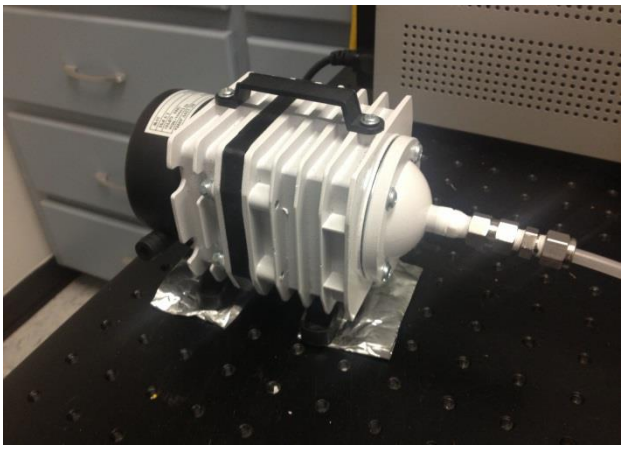

Figure 12. Air pump used in the experiment.

Before the air can reach the inlet to the pebble-bed heater, it needed to have several safety, control, and measurement devices. First, the pump did not have an on/off switch, so the system needed an easy-shut-off ball valve (Figure 13) in case the air supply needed to be stopped at any time. Secondly, there had to be a needle valve (Figure 14) to control the amount of air flow with changes in small increments to reach a precise flow rate as this would be one of the three main variables in the study. Finally, a flow meter (Figure 15) would have to be installed downstream of both valves to monitor the volumetric flow rate of the air entering the heater. The needle valve and ball valve were purchased from Swagelok, and the flow meter was already in the lab [69,70]. The flow meter could be recalibrated easily to define zero flow and even be programmed to measure the volumetric flow rate of several different gases, but for this experiment it was only set to measure air.

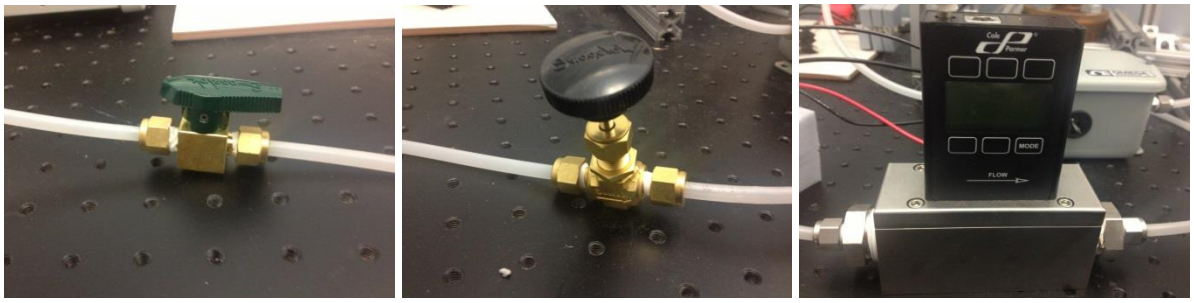

Figures 13, 14, 15. Ball valve, needle valve, and flow meter.

For each tubing connection to the air pump, valve, flow meter, or the main device there would need to be a female fitting that could attach to the tube, secure the tube to its target, and make an air-tight seal. Swagelok had female 0.635 cm (1/4”) tube fittings that would be screwed on to the end of each piece of tubing, so that it could mate with any of the previously mentioned connections. These fittings came in brass and stainless steel, so either brass or stainless steel was used depending on what metal the particular tube was connecting to.

The air would need to be sent through the heater vertically from bottom to top. For air, if the flow entered from the top, then the mixed convection would be affected and the net velocity decreased. The heat escaping the pebbles would rise and slow the flow of the fluid. For liquid, if the heater was run horizontally, then the liquid would only run through the lower half of the pebbles. Therefore, the heater would be built vertically with the air entering the base, so that this device could be experimented with liquids in the future without any modifications.

Now that the air has been supplied, all tubing connected, and the speed regulated, it can enter the base of the pebble-bed heater. For this connection to exist, another copper disk would have to be made by the machine shop for the very top and the very bottom of the pebble-bed heater in order to provide a means of screwing in a fitting on both ends to connect the air tubing with the heater’s inlet and exit. The fitting on both ends would need a simple 0.635 cm (1/4”)

brass male to female fitting. The male side would have NPT (National Pipe Thread) threading so as to achieve a more air-tight seal against the copper disk, and the other side of the fitting would be equipped to screw into the 0.635 cm (1/4”) female fitting on the end of the tube. The end disk would be 2.54 cm (1”) thick and have the 0.635 cm (1/4”) NPT threaded hole cut out on one side 1.27 cm (1/2”) through and then a straight hole would be made the rest of the way. The disk would also need the four holes 90° apart for the bolts to secure the end piece to the rest of the device. Figures 16 and 17 show the design of the end disk that the machine shop was to follow when tooling the copper. The two brass fittings were ordered from Swagelok, and the 10.16 cm (4”) copper material was purchased by the machine shop [72].

Since the air tubing entering the base had a 0.635 cm (1/4”) diameter, and the pebble chamber surrounded by the work coil was 2.54 cm (1”), something would have to be added on the front end of the heater in between the two to normalize the flow and make it more uniform over the cross-section before the air reached the pebble bed. This addition would need to be placed after the bottom disk where the air entered and before the first disk containing the two measuring instruments. To best break up and normalize the flow upon entry, a wad of metal

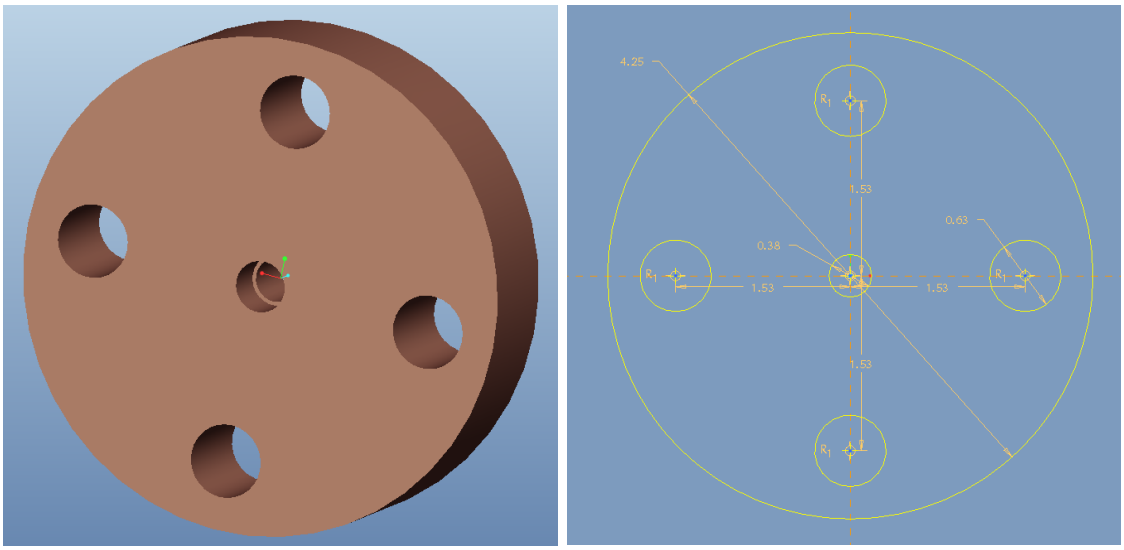

Figures 16 and 17. The design for the copper end disk spacers.

wool (Figure 18) inside a short pipe segment seemed to be the best option. The pipe would again be 2.54 cm (1”) copper pipe and have a copper flange on either end to connect to both copper disks. To be consistent, it was decided that there should also be a metal wool pipe segment after the heating process, so that the air would flow past the second set of instruments in the same way as the first. The copper pipe and flanges were purchased in the same shipment mentioned previously, and the bronze wool was found at Home Depot [29]. Since the holes in the flanges were 1.588 cm (5/8”) in diameter, and there were now four sets of four bolts needed for the flanges and copper disks; sixteen 1.588 cm (5/8”) diameter, 5.08 cm (2”) long bolts were also ordered from Home Depot along with the bronze wool from earlier and the nuts to go with the bolts.

Figure 18. Bronze wool for normalizing the flow of air.

For the steel balls that would make up the pebble matrix, several different sizes would be considered, since it was decided that the pebble size would be one of the variables in the experiment. The difference in pebble size would reveal if the volume or surface area of metal played a role in the exit temperature of the air. First, in order to get more heat out of the steel

balls, carbon steel was chosen over stainless steel as the material. Carbon steel and stainless steel are both comprised of mainly carbon, iron, and several trace amounts of other materials. However, stainless steel's iron content is closer to 50%, where as carbon steel can have as much as 98% iron. Since carbon steel has more iron, it would be more affected by the hysteresis loss effect. The pipe segment would only be 2.54 cm (1") wide, so carbon steel balls smaller than 1.27 cm (1/2") were considered. In order to get a large enough number of pebbles, 0.635 cm (1/4"), 0.476 cm (3/16"), and 0.318 cm (1/8") were chosen for the three sizes, and the difference between the spheres can be seen in figure 19. Carbon steel ball bearings were available in the desired sizes, so the three sets of ball bearings were purchased from MSC Industrial Supply [40]. As the diameter of the balls decreases, more balls would be needed to fill the same space; therefore, the number of ball bearings which was ordered increased as the diameter decreased: 500 of the 0.635 cm (1/4"), 1000 of the 0.476 cm (3/16"), and 2,500 of the 0.318 cm (1/8").

Figure 19. Carbon steel ball bearings: 0.635 cm (1/4"), 0.476 cm (3/16"), 0.318 cm (1/8").

Once the steel ball selection had been made, it was decided that there would have to be a wire grate or wire mesh before and after each segment to prevent the steel balls and even the wire wool from moving between the sections of the pebble-bed heater. The wire mesh would still

allow the air to flow through unobstructed. It had to be strong enough to support the weight of the pebbles and have small enough holes so that the 0.318 cm (1/8”) balls could not slip through. After searching several stores, some aluminum wire mesh (Figure 20) was found at Hobby Lobby with 0.159 cm (1/16”) holes that were small enough to not let anything but air pass through [28].

Two thermocouples would be needed for the experiment; one above and one below the pebble matrix. As mentioned previously, the thermocouples would come in through the side of the middle copper spacers and be held by brass fittings. Thermocouples come in several different models or “types”; each type is capable of reading different temperature ranges and serving

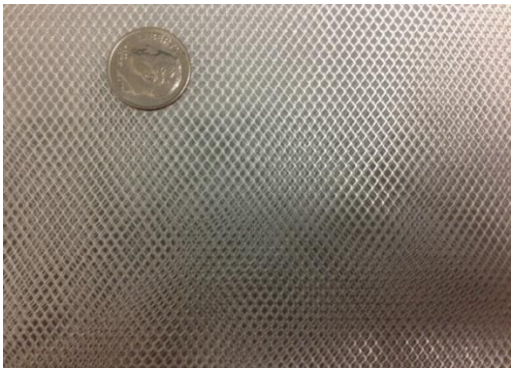

Figure 20. Aluminum wire mesh with 0.159 cm (1/16”) holes.

unique functions. Originally, K-type was considered, since it had the most favorable temperature range for the experiment, capable of reading up to 1,523 K (2,282 °F). Once it was learned that K-type thermocouples did not function inside magnetic fields, they could no longer be used [50]. Instead, T-type thermocouples (Figure 21) were found to be a suitable substitute. T-type could only read up to 623 K (662 °F) but were unaffected by magnetic fields, so they were the best option for the small-scale testing in which temperatures were not going to be close to the maximum reading temperature [50]. Using Omega’s selection guide to choose the proper

thermocouple, two T-type thermocouples were purchased [51]. In order to reach the center of the air flow, the thermocouple should have at least a 15.24 cm (6”) long probe. The two thermocouple fittings would come from Swagelok. The fittings needed male NPT threading on one end to securely fasten to the copper disk, a female connection on the other end to secure the thermocouple, and the interior to be “bored through” so that the thermocouple could pass through the fitting [71].

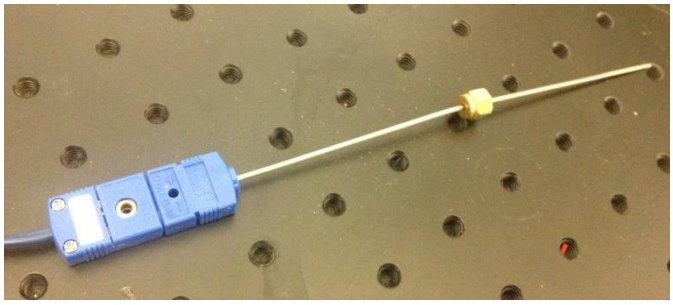

Figure 21. T-type thermocouple with 15.24 cm (6”) probe.

In order to read the temperature value from the thermocouple, the millivolts could be read from the two wires coming out of the instrument using a digital multimeter (DMM). The voltage would then be converted to a temperature using the T-type thermocouple reference tables [52]. The thermocouple’s wires could also simply be hooked up to a thermocouple reader, which would take care of all conversions and display the temperature value. To avoid the hassle, time, and potential error from the conversion technique, the thermocouple reader method was chosen. The lab owned several thermocouple readers with different capabilities. The reader selected for the experiment, which can be seen in figure 22, had the ability to measure up to 10 thermocouples, read different “types” of thermocouples, and calibrate using an ice bath.

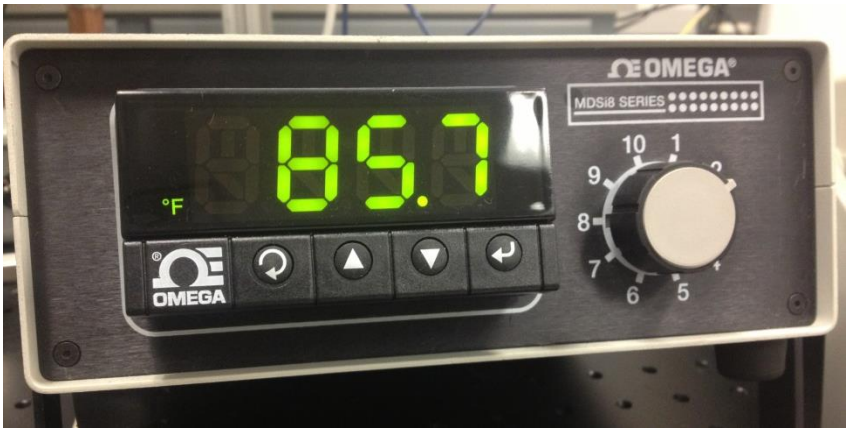

Figure 22. Thermocouple reader.

In addition to temperature, the pressure difference was also to be measured. To accomplish this, a differential pressure transducer (DPT) was to be used. The lab owned the DPT in figure 23, which was capable of measuring changes in air pressure. It had a port on either end to which a pipe or tube could be attached. This DPT would need to have some of the 0.635 cm (1/4") low-density polyethylene clear air tubing attached to each of the two ports—one to measure the higher pressure and one for the lower. The lower temperature port would connect to the spacer before the heating, and the higher temperature port would connect to the spacer after the heating, since the pressure would increase as temperature increased. At each connection to a spacer, there would be another bored-through, male NPT threaded fitting to allow the tubing to pass through the fitting and read from the middle of the flow [73]. In order to read the difference in pressure, a digital multimeter would have to clip onto the two output wires of the DPT. Next, the displayed voltage on the multimeter would be converted to difference in pressure in units of Pascals (Pa=N/m^2) using equation 3, which was derived from the instrument's user manual [49].

$$\Delta P\ [\mathrm{Pa}] = 8{,}618.45\left[\frac{\mathrm{Pa}}{\mathrm{V}}\right] * (\mathrm{V}\ [\mathrm{V}] - 1) \qquad \text{Eq. 3}$$

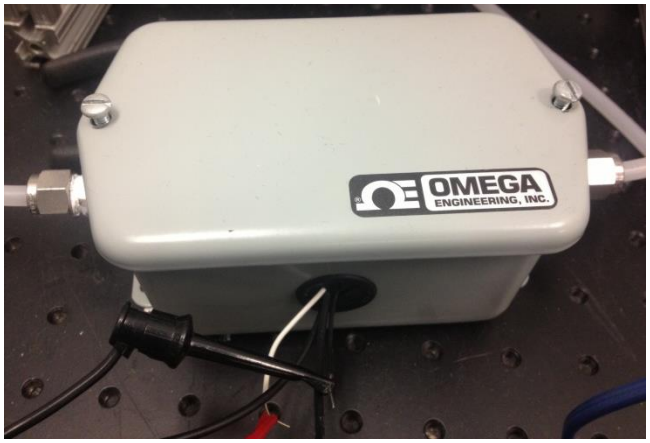

Figure 23. Differential pressure transducer with DMM clips attached to output.

After both the pebble-bed heater and induction heater had been built, an issue arose with the copper pipe center section. The induction heater would short out every time the copper work coil touched the copper pipe or any metal object. To resolve this insulation problem, the pebble chamber and its two flanges would no longer be made out of copper and instead were designed as one solid unit in Solidworks as seen in figure 24. Proper thickness was given to the pipe walls, so the material was sturdy and strong enough to support the load of weight above it. The design of the printed piece would be the exact same dimensions as the copper version, except that it would be made as one solid piece to minimize the possibility of air leaks and weak points. Three of these units were successfully printed using ABS plastic material at The University of Alabama's 3D Printing Lab. The main disadvantage of the ABS plastic is that it transitions from a hard plastic to a rubbery plastic at 377 K (219 °F), which means that high temperatures cannot be achieved with this part as the pebble chamber [68]. This was intended to be a temporary fix, so that experiments could be run, not a permanent solution to the magnetic induction pebble-bed heater. The permanent solution is covered in the Discussion section later in this paper.

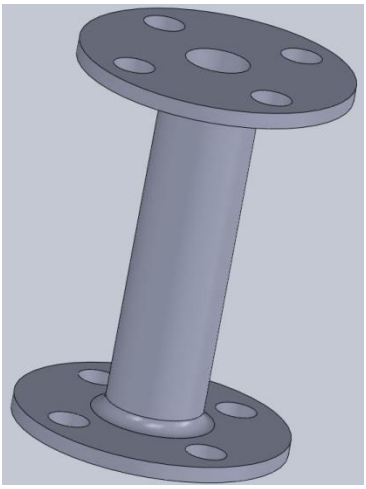

Figure 24. Solidworks drawing of pipe and flange assembly.

Finally, after designing and giving careful consideration to each aspect of the pebble-bed heater and having acquired all the parts and tools necessary, the construction of the pebble-bed heater could begin. The pneumatic schematic of the system can be seen in figure 25.

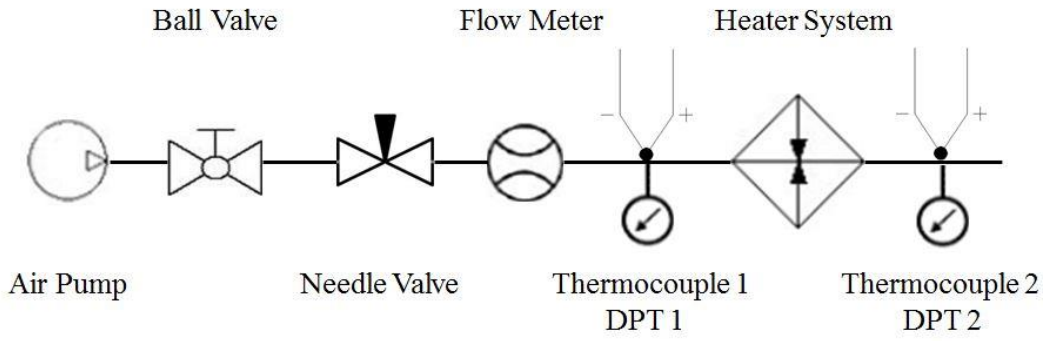

Figure 25. Schematic of the pebble-bed heater experiment.

B) Constructing the Pebble-Bed Heater

Before construction could begin, the two copper flange-pipe-flange sections for the wire wool needed to be sweated together by The University of Alabama's machine shop. The sweating process would not only secure the pipe to the two flanges, but it would also make the connection air-tight.

For the next step of the preparation process, the aluminum mesh was cut to make six different circles that were slightly larger than the 2.54 cm (1”) hole. Then, six cardboard cutouts had to be made. The cardboard would act as a washer preventing air from leaking out of the gap made by the thin wire mesh as well as a means of securing the aluminum mesh circles to the different parts of the assembly. The cardboard was cut the same way as the flange. It had a 2.54 cm (1”) hole in the center, 10.8 cm (4.25”) outer diameter, and four equidistant 1.588 cm (5/8”) holes for the bolts. Using cyanoacrylate (Krazy Glue), each piece of aluminum mesh was adhered over the center hole in each of the cardboard cutouts.

With all parts in hand and all preparation work finished, the heater construction began at the start with the air pump. The air pump did not require any assembly or wiring, but it did need to be secured to the table, since it would vibrate and move while turned on. The air pump had holes in its legs that would allow it to be screwed down; however, the spacing of the screw holes did not fit with the table that the experiment was being conducted on. Therefore, the air pump was kept in place by putting tape underneath it.

Seven pieces of air tubing were then cut and female fittings secured to each end. Three short pieces were cut to be less than 15.24 cm (6”) long, three medium pieces were cut to be about 30.48 cm (1’) long, and one long segment was made to be almost 60.96 cm (2’) long. With the first short piece, one end was tightened onto the air pump’s exit, and the other was attached to the ball valve. Plumbing tape was used on every fitting connection in the entire setup to ensure that air could not easily escape through the grooves. Another short piece of tubing was placed between the ball valve and the needle valve, and the third was fastened between the needle valve and the flow meter. The long cut of tubing connected the flow meter to the fitting at the base entrance of the pebble-bed heater. Finally, a piece of padding was placed under the ball valve

and needle valve to reduce vibration noise caused by the air pump. Figure 26 shows the entire initial configuration prior to the pebble-bed heater.

Figure 26. Experiment configuration from air pump to flow meter.

The fitting at the base was screwed into the NPT threaded hole on the underside of the bottom copper disk. Next, the copper pipe with the metal wool was to be installed to help make the flow uniform. A small wad of the bronze wool was stuffed inside one of the small flange-pipe-flange sections but not compacted enough to restrict airflow. A piece of aluminum mesh and cardboard was adhered to the outer side of each flange preventing the wool from interfering with other parts of the heater. One of the flanges was then secured to the copper base using four of the bolts. The progress can be seen in figure 27.

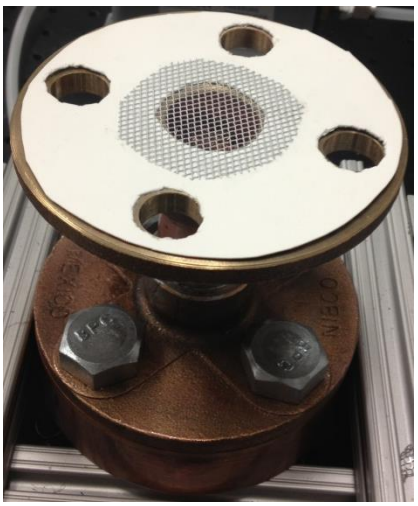

Figure 27. Construction up to the first pipe section.

Next, the first middle copper spacer would be installed. In addition to simply being placed atop the flange, the first thermocouple probe and low-pressure DPT tube needed to be installed in the side. After being wrapped with plumbing tape, the thermocouple and tube fittings were tightened into the side wall. The thermocouple probe was pushed through the fitting and fastened to the fitting once the probe was in the center of the inner 2.54 cm (1”) hole. The same process was done for the DPT tubing after two of the medium length tubing sections were fixed to either port on the DPT. Both fittings are shown in figures 28 and 29.

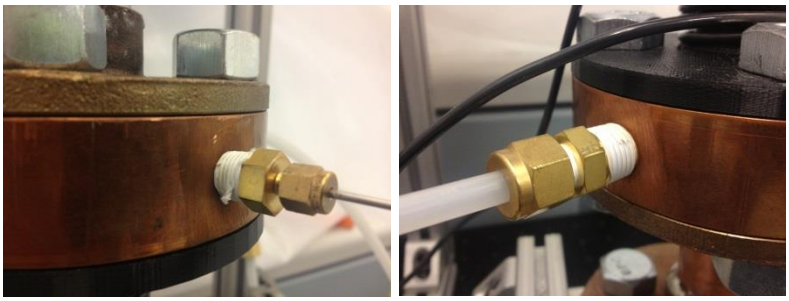

Figures 28 and 29. Thermocouple probe and DPT tube attached to the copper spacer.

After everything had been attached to the first disk, the 3D-printed, ABS plastic center section would follow. Another aluminum mesh and cardboard part was glued to the base of the plastic pipe, so that the ball bearings would not fall out of the bottom. The first set of ball bearings loaded into the pebble chamber was the 0.635 cm (1/4”) carbon steel balls. The ball bearings were counted as they were loaded into the pipe, and it took 300 of the 0.635 cm (1/4") size to fill the 15.24 cm (6”) long pipe. Once full, the chamber was bolted to the disk and bronze wool pipe section below. Figure 30 shows the development of the experiment up until this stage.

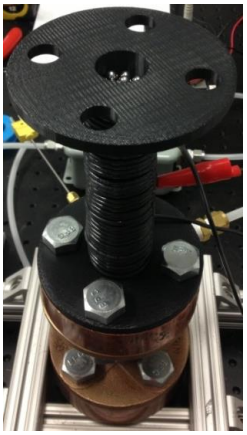

Figure 30. Construction up to the main center chamber.

The fourth cardboard cutout was then attached to the under-side of the second copper disk instead of the top of the 3D printed pipe, so that the ball bearings could be emptied and filled. The two fittings were tightened into the second middle disk, and then the second thermocouple probe and high-pressure DPT tube were attached in the same way as before in order to read from the middle of the 2.54 cm (1”) hole where the air would be flowing.

The second wad of bronze wool was stuffed inside the remaining short copper pipe, and then the last two cardboard and aluminum mesh pieces were adhered to the outer side of each flange to contain the bronze wool. One of the copper flanges was then bolted to the copper disk and plastic flange.

For the final part of the main pebble-bed heater construction process, the second outer copper disk was placed atop the remaining flange, and the last set of four bolts tightened them together. A 0.635 cm (1/4") tube fitting with NPT threads was screwed into the hole on the top of the disk, so that the third medium length piece of air tubing that was cut in the beginning could be attached to the exit of the pebble-bed heater. The exit hose was necessary, so that hot air was not leaving the system in an uncontrolled manner. The air could now be directed to a safe area.

In the event that a liquid is used instead of a gas in future testing, this would also provide a means of depositing the liquid into a bucket or sink.

Once the heater was finished being built, it needed a way to stand vertically and not be knocked over easily. The lab had a large collection of extruded aluminum frame pieces and connectors, so a stand would be made out of that to hold the heater vertically [80]. The rods are square 2.54 cm (1”) by 2.54 cm (1”) rods of various lengths. The pieces can be attached to each other easily in any direction using only the supplied joints, fasteners, and an allen wrench making it ideal for creating a customized stand. The base of the heater needed to be about 5.08 cm (2”) off of the ground, so that the air tube and fitting would have enough room to come up and enter the bottom. The rods were spread wide at the base to prevent tipping. Then, a second layer perpendicular to the first was set closer to the center for the heater to rest on. The gap between the two rods was barely wide enough for the bolts at the base to fit between. A third layer was set perpendicular to the second layer—parallel to the first—with the rods 10.16 cm (4”) apart, so that the device would have a very tight fit to keep it from wobbling. Then, several longer rods were stood vertically at the four corners and connected to one another, so that the pebble-bed heater could not easily be hit and knocked over. The vertical stand and pebble-bed heater were now complete as seen in figure 31 with only a few minor steps left.

In addition to the main construction, the thermocouple reader and differential pressure transducer needed to be set up. The thermocouple reader had the ability to measure up to 10 different probes, so there were 10 locations for thermocouples to attach in the rear. The two copper-constantan thermocouple wires were screwed into the first two ports of the device as seen in figure 32. The #1 thermocouple was the upstream probe before the matrix, and the #2

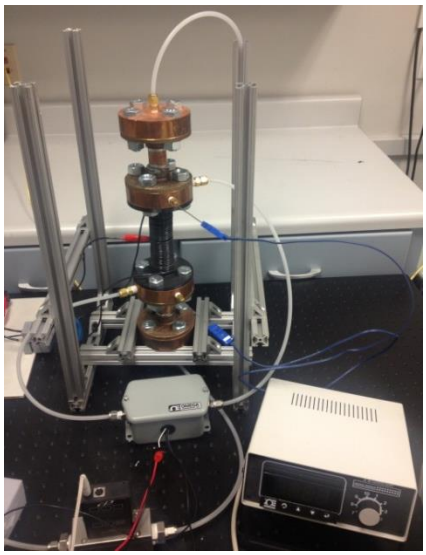

Figure 31. Completed stand and pebble-bed heater.

thermocouple was the probe after the heating had taken place. Once the instruments were connected to the machine, the probes were submerged in an ice bath for ten minutes in order to calibrate the device to 273 K (32 °F). After calibration, the probes were reconnected to their respective places in the pebble-bed heater.

Figure 32. Rear of thermocouple reader with thermocouples connected to ports 1 and 2.

The differential pressure transducer required some wiring before it could be used. The lid was unscrewed, and a 250 ohm resistor was added between terminals 2 and 3 as shown in figures 33 and 34, so that the device would output the pressure reading in volts instead of amps. The 250 ohms was reached using four 100 ohm resistors in a combination of series and parallel. To calibrate the DPT, both the high pressure and low pressure ends were stopped up, so the pressure would be the same on either end with no velocity or temperature difference. Once the pressure difference was zero, the calibration potentiometer on the far left side of the DPT was twisted until the output read 1 volt (1 V = 0 Pa, see equation 3). The lid was re-attached, and the tubes were placed back inside the heater.

A complete step-by-step process of the construction is pictured in the Appendix. The pebble-bed heater portion of construction was now fully complete, and the induction heater design process could begin.

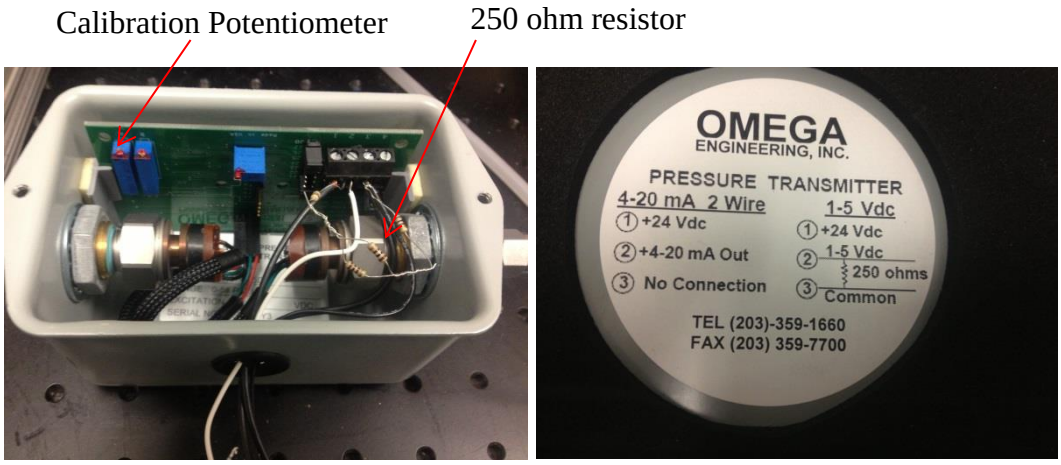

Figures 33 and 34. The internal wiring and wiring diagram of the DPT.

C) Designing the Induction Heater

The design of the magnetic induction heater in the experiment began with finding a practical schematic. The wiring design had to be powerful enough to provide the necessary heat,

but not so complex that it could not be easily reproduced. The schematic chosen for the pebble-bed heater would come from www.RMCybernetics.com [61]. The design was very simple yet powerful and only required nine main parts along with a power supply unit. The schematic was modified to add more detail and can be seen in figure 35. This circuit is called a collector resonance oscillator circuit. It is both simple and self-resonating, so it will automatically run at the resonant frequency determined by the capacitors and work coil [61]. While this circuit was practical for a small-scale, low temperature test, it would not be suitable for a bigger scale with larger amounts of metal or if a temperature above 533 K (500 °F) was desired.

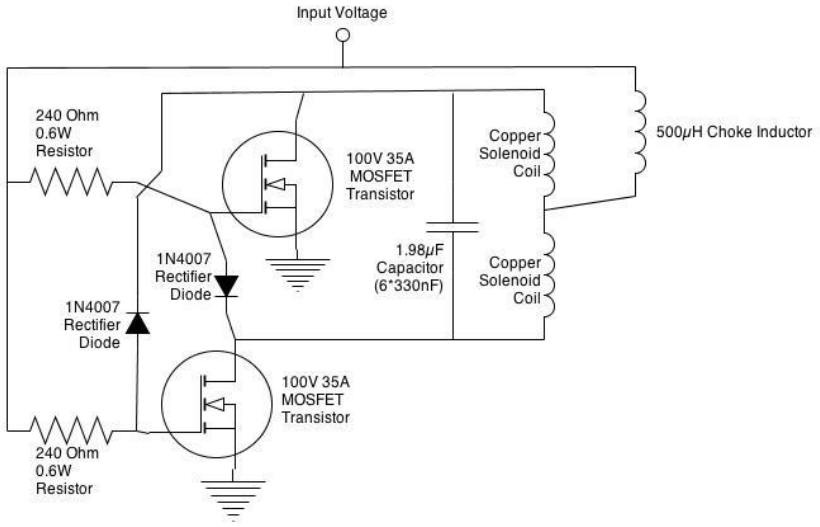

Figure 35. Schematic of the induction heater used in this experiment.

The first major component was a DC power supply unit. The power supply needed to be capable of providing up to 15 volts and 5 amps and delivering a large surge of current at start up. In addition, the voltage and current level had to be easily adjustable, since the amount of power delivered to the coil would be the third variable in this study. There were a number of available power supply units in the lab. Although, several devices were incapable of being adjusted, some

lacked a display, and others did not deliver a high enough voltage. The one shown in figure 36 was capable of meeting all the needs and therefore chosen for the experiment.

The next aspect of the design process was determining the specific electrical components necessary to create the induction heater as these details were not included in the original schematic. The parts included a work coil, a choke inductor, six capacitors, two resistors, two diodes, and two transistors.

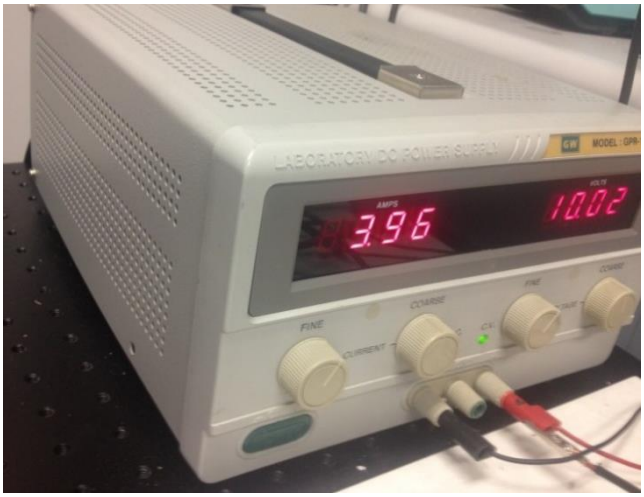

Figure 36. DC power supply with electronic display and adjustable voltage.

The coil for this schematic was required to be a solenoid with a center tap—a location for current to enter at the middle of the solenoid. Different coils were considered and tested to find the best fit. The solenoid would need to be made of a conductive material that was thick enough to handle the large amounts of current. This meant that the coil could either be a thick wire or a small pipe, and the material would be brass or copper. Brass was dismissed once it was found to deform at high temperatures, which meant copper was to be the solenoid material [61]. Soft copper pipe worked quite well as a work coil. It was easy enough to bend and wind into shape so

that it had the desired inner diameter to fit around the pipe. The pipe was able to withstand high frequency currents better than a wire, as the current would flow around the outside of the pipe instead of building up a resistance. If cool water was run through the center of the pipe, then it could tolerate even higher power levels and temperatures.

Unfortunately, the only soft copper pipe found was uninsulated and the circuit would short if any metal touched the coil, so a thick, insulated, copper wire was the final solution. While the wire would be thinner than the pipe and unable to carry as high of a current, it would allow the solenoid to have more turns per unit length, which would increase the density of the magnetic field. Using a wire selection guide, gauge 12 wire was chosen, since it could handle the 5 amp current for a longer distance than was necessary and was still easy enough to bend into shape [23]. The gauge 12, copper, solid-core wire for the solenoid was cut in a 6.096 m (20’) long segment from the lab.

The current would first be supplied to the solenoid at its center, but before the current could reach the center tap of the solenoid, it must pass through an inductor, referred to as a “choke inductor.” Choke inductors range from less than one microhenry (μH) to several hundred millihenries. Its purposes include preventing the high frequency oscillations from entering the power supply and keeping the current at a reasonable level [61]. The choke inductor will therefore increase the lifespan of the system and reduce maintenance. Just like the work coil, the choke inductor would need to be made of a thick enough gauge wire to handle the high levels of current being supplied to the solenoid. Another factor to consider is that in an induction heater system, the choke inductor needs to have a reasonably high inductance of several hundred microhenries to block the high frequency oscillations, so a 500 μH choke inductor made of thick wire was purchased from Mouser Electronics and can be seen in figure 37 [39].

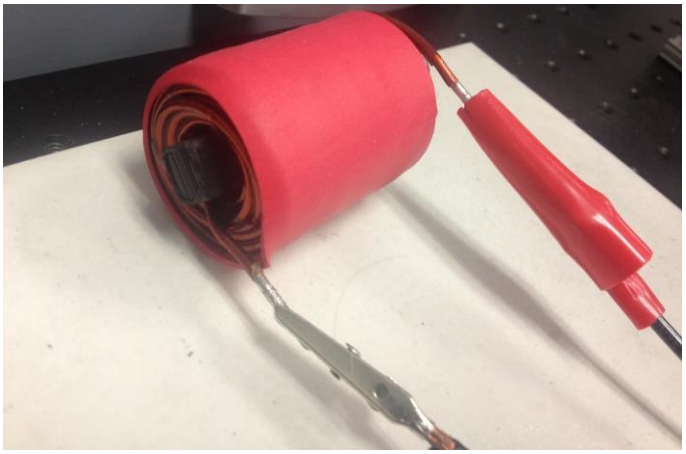

Figure 37. 500 µH choke inductor.

Looking at the schematic, there is a capacitor in parallel with the work coil creating a resonant tank circuit thus generating a resonant frequency within the system. Instead of having one large capacitor, it would be better to distribute the current and heat among more capacitors, so that, as a whole, the capacitors could handle a higher power level and be less likely to fail. Therefore, six 330 nanofarad (nF) capacitors were combined in parallel to each other and with the solenoid to reach 1.98 microfarads, which would reduce the resonant frequency to a safe level (21.74 kHz) according to RMCybernetics [61]. After searching online, 1 kV, 330 nF, polypropylene capacitors were found from Digikey (Figure 38) [13].

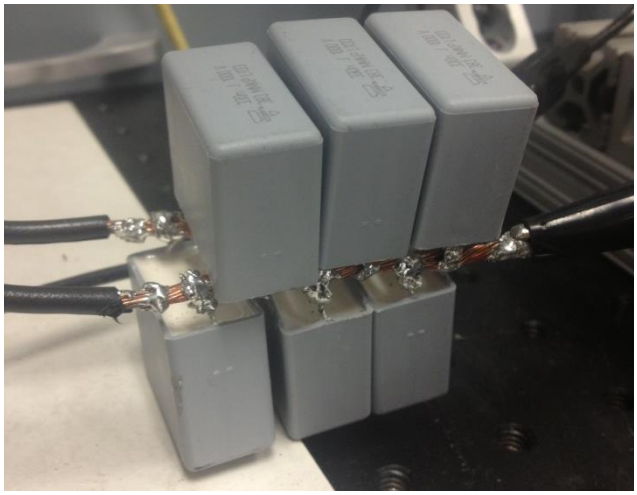

Figure 38. Six 330 nF capacitors combined in parallel with each other and the work coil.

The voltage and current also enter the circuit through two resistors. Their resistance determines how quickly the transistors will turn on and should therefore be a relatively low amount. Although, if the resistance is too low, the resistor would be pulled to ground by the diode when the opposite transistor is active, so the resistance should be lower than 500 ohms but not below 100 ohms [61]. 240 ohms was determined to be a safe value, and the appropriate resistors were purchased from www.RMCybernetics.com [62].

The two diodes in the circuit are responsible for discharging a transistor, while the other transistor is activated. In order to drain the transistor quickly and completely, the diode selected should have a low forward voltage drop and a quick response time. The diode should also be able to handle high surges of voltage and prevent a reverse flow of voltage. Schottky diodes were considered, since they are known for having a low forward voltage drop and rapid switching speed [24]. More specifically though, a Schottky rectifier diode was chosen for the circuit, since it was better equipped to prevent reverse voltage flow than a standard Schottky diode [24]. The rectifier diodes were purchased from Digikey [11].

The final electrical element to the circuit was the transistors. The two transistors would be activated by their resistors and drained by the diodes, and the transistors themselves would be responsible for alternating the flow direction of current in the work coil. The specific transistor model chosen would need to be capable of functioning at the frequency determined by the capacitors and be rated for at least five times the voltage and current that the circuit will be supplied with. MOSFETs (Metal-Oxide Semiconductor Field-Effect Transistor) were chosen due to their low drain-source resistance and fast response time [74]. This would allow them to both drain and turn on/off quickly. A large number of these transistors would need to be ordered,

since they are the piece that short circuits easily. They would burn up if anything was wrong with the circuit or if any metal touched an uninsulated part of the work coil. The transistors can also decline in performance after twenty to thirty hours of use and would eventually need to be replaced. The MOSFETs were ordered from Digikey along with the diodes and capacitors [12].

Since the MOSFETs were likely to get warm during testing due to the long tests and the high operating frequency, it was necessary to get a heat sink for each transistor. The transistors had a hole in them for a small screw, so the heat sinks needed to have a small hole of the same size. As shown in figure 39, this would hold the transistor to the heat sink for a good connection, allowing the heat to easily transition to the heat sink. A suitable heat sink was found on Digikey, and one was purchased for each transistor [14].

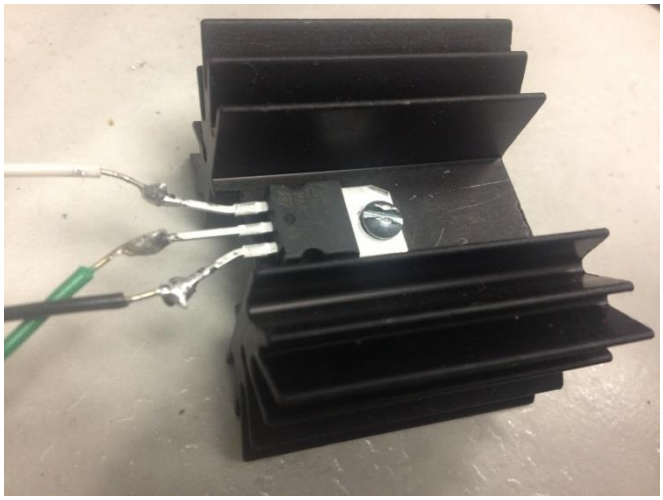

Figure 39. MOSFET and heat sink.

Typically, a solderless breadboard would be used to hold the circuit and connect the pieces to one another. Since the circuit would be using up to 5 amps and the lab only had breadboards capable of handling up to 1 amp, the circuit would have to be built as a floating circuit. This meant that the wires, resistors, diodes, etc. would not be plugged into anything. The

wires would simply be twisted or soldered to one another. To make the floating circuit somewhat more secure, 10 amp alligator clips and several plastic twist nuts were used to help with connections.

D) Constructing the Induction Heater

The work coil took several attempts before a suitable center-tapped solenoid was made. The first efforts involved a 0.847 cm (1/3") soft copper pipe and then the 12 gauge wire. The first attempt with the pipe was a failure, but the second solenoid was made as one solid unit and several turns longer than the first. The pipe was easy enough to bend into shape around the outer diameter of the pebble chamber. The wire connecting the solenoid to the choke inductor could either wrap around a point at the center of the coil or be soldered to the same point. Soldering was not as easy on the pipe, so a ring of solder was made around the pipe. Next, the wire from the choke inductor was inserted into the solder. The end result, seen in figure 40, was a success and would have been used in the final experiment if it had been better insulated. If the copper coil ever touched a piece of metal while the power supply was on, the transistors would burn up and need to be replaced.

Figure 40. Solenoid made from copper pipe.

Finally, the 12 gauge solid-core wire was used to make the solenoid for the induction heater. The 6.096 m (20’) long section was wound 35 times around the center section of the pebble-bed heater with a final coil length of close to 12.7 cm (5”). The end result is pictured in figure 41. There was enough leftover wire on either end to extend down to the surface near the circuit so that the wires could eventually be attached to the capacitors. Since the center pipe would need to be removed from time to time to change out the ball bearings, there could not be any permanent connections to the induction heater circuit. Therefore, alligator clips were put on either end of the wire used to make the solenoid, so it could easily be detached and re-attached. Using a scalpel, a slit was cut in the wire’s insulation half of the way down the solenoid, so that a connection could be made for the center tap.

A 10 amp alligator clip was fixed to either end of two short pieces of 12 gauge wire. For the first wire, a clip was attached to the incision made in the induction coil, while the other was clamped to one end of the choke inductor. The second wire was used to connect the other end of the choke inductor to the output of the power supply unit.

Figure 41. The final coil for the induction heater.

The next step was to install the capacitors. For best results, the capacitors should be placed as close as possible to the solenoid. In order to secure each of the six capacitors to either end of the coil's wire, a short segment of 12 gauge, multi-strand wire was used. Since the wire was multi-stranded, the legs of the capacitors could easily be run directly through the middle of the wire, wrapped around, and soldered for a permanent connection. This was done for each of the capacitors until all six were in parallel. In order to give the clips from the solenoid a good grasp on the multi-strand wire, the end of both multi-strand wires going to the coil were covered in soldered. Alligator clips were attached to the other ends of the wires going towards the circuit.

Before the circuit could be built, some research into MOSFETs had to be conducted. The MOSFETs had three legs called the gate, source, and drain. If looking from the front side, the gate was on the left, drain in the middle, and the source on the right for the particular MOSFETs purchased [66]. If the transistor was "On," then the voltage would enter the gate, opening a connection between the drain and source. This connection would provide a pathway for the voltage from the work coil and the voltage intended for the "Off" transistor to be grounded [74]. The transistors would then flip roles; the transistor that was "Off" was now "On" and vice versa. This would cause the opposite transistor to act as the ground for the work coil compared to before reversing the direction of the current and the magnetic field. This process would happen as many times per second as the frequency of the resonant tank circuit.

Before any wiring took place, the MOSFETs were first fixed to their heat sinks using a small screw and nut. A wire was then soldered to each of the three legs to give it additional length. A cable was run from the output of the power supply to a wire, which was connected to the two resistors by a twist nut. The other end of each resistor was then connected to both the

upstream side of a diode and the gate of a MOSFET using a twist nut. The downstream side of each diode was then connected to the drain of the opposite MOSFET. The source legs of each MOSFET were connected to each other with a twist nut and then connected to the ground of the power supply by a cable. Finally, an alligator clip coming from each capacitor wire was clamped to the downstream side of one of the diodes. Without a breadboard and with so many junctions, the end result of the circuit was a bit clustered, as seen in figures 42 and 43, but functioned perfectly.

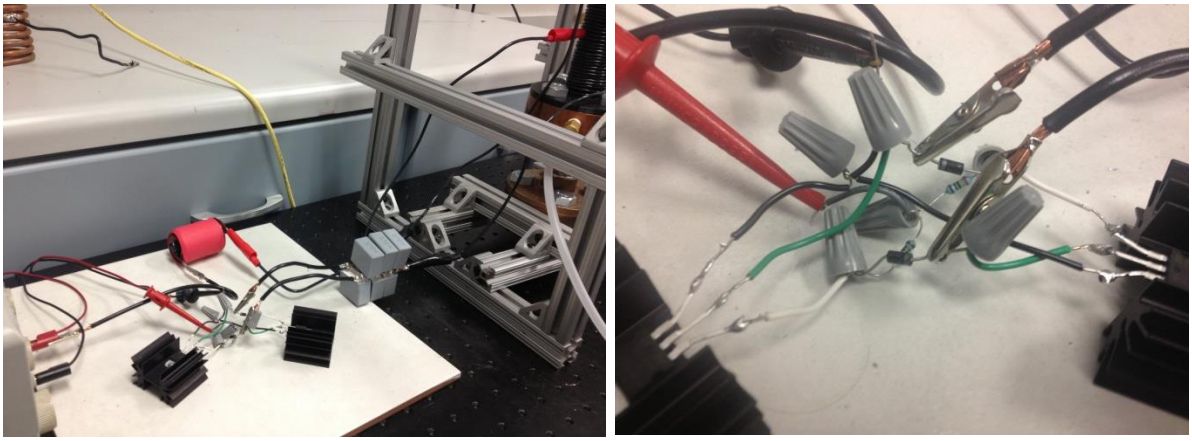

Figures 42 and 43. Induction heater circuit and wiring.

To verify that the induction heater was functioning, a screw driver was inserted inside the solenoid for 30 seconds. After removing the screwdriver, the temperature was measured using an infrared thermometer, and it was found to be over 366 K (200 °F). A paper clip was then entered into the same magnetic field was close to 478 K (400 °F) after the time period. This simple test proved that the induction heater indeed worked.

CHAPTER 4

TESTING PROCEDURE

As mentioned previously, the experiment of the small-scale magnetic induction pebble-bed heater would be subjected to numerous tests involving different combinations of pebble sizes, flow rates, and power levels. There would be tests run at three different voltages, flow rates, and pebble sizes with every combination possible. Therefore, 27 total experiments would be conducted, and they would be completed in sets of three to minimize strain on the system. To reduce the time between tests, the pebble size would only be changed after the 9 tests with the current pebble size had been run. The reason being, it would take more time to change the pebble size than it would to adjust the knobs and valves for the power supply and flow rate. The three pebble sizes were 0.635 cm (1/4"), 0.476 cm (3/16”), and 0.318 cm (1/8”). In order to avoid reaching high temperatures that would melt the plastic pebble chamber, 10 volts would be the highest voltage applied to the system. The three voltage levels would be 5, 7.5, and 10 volts. The air pump had a maximum flow rate of 20 liters per minute (LPM), so the flow rates would be 10, 15, and 20 LPM. During a performance test with the air pump, the max flow rate from the air pump would drop about 2-3 LPM after an hour of testing. Consequently, the higher flow rates were always tested first.

The first set of ball bearings would be the 0.635 cm (1/4”) diameter set. After filling the pebble chamber to the brim, it was found that 300 of the balls could fit inside. Once loaded, the pebble-bed heater was bolted back together. Prior to each test session, the air pump and induction heater would be shut off, so the DPT and flow meter could be set to zero in order to improve the accuracy of the results.

The first set of three experiments would be run at 20 LPM, and the three different voltage levels would be applied in increasing amount. By increasing the voltage between tests instead of decreasing, it would eliminate unnecessary time waiting for the system to cool back down. Once the max temperature was reached at the first voltage, the voltage would be increased to the second level, and the temperature would rise from the end of the previous test. The same would be done for the third voltage. The current provided to the circuit was automatically adjusted by the circuit and the power supply. The current was dependent on the surface area of metal inside the solenoid and the voltage level. Equation 4 shows the voltage-current relationship for the 0.635 cm (1/4") carbon steel balls as determined by the linear relationship in figure 44, accurate to within 0.05 amps.

$$\mathrm{I\ [A]} = 0.4388 \left[\frac{\mathrm{A}}{\mathrm{V}}\right] * \mathrm{V\ [V]} \qquad \text{Eq. 4}$$

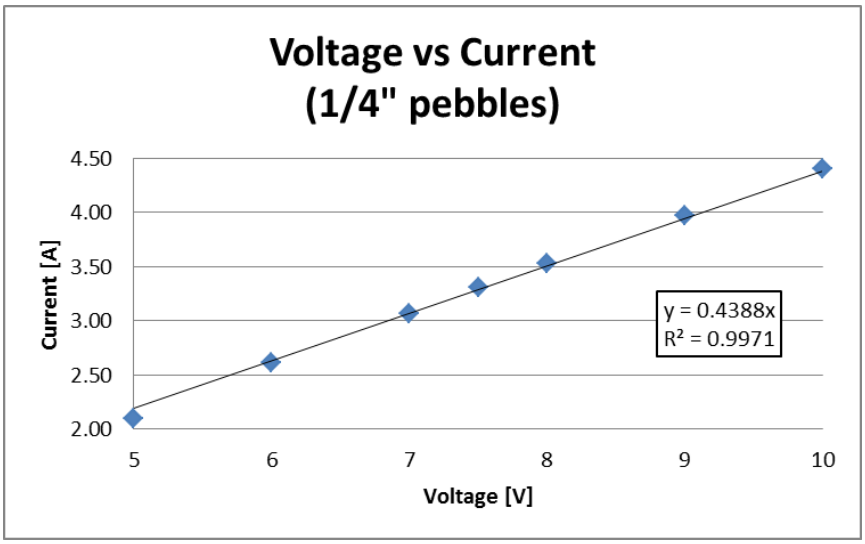

Figure 44. Voltage-current relationship for 0.635 cm (1/4") balls.

At 20 LPM the air would reach 90% of the maximum temperature after 10 minutes, but it would take approximately 20 total minutes before the exit temperature of the air would stop

changing. After the 5 volt test had stagnated, the temperatures and change in pressure were recorded. The voltage was then increased to 7.5 volts for another test and again to 10 volts once the second test was finished. After the three tests had been run, the system was turned off to allow it time to cool and rest. The next set of three tests would be conducted the following day for ample recovery time.

With the 0.635 cm (1/4") pebbles still inside, the needle valve was adjusted to decrease the flow rate to 15 LPM, and then the three voltage levels were tested in the same order as before. After the temperature and pressure readings were recorded for each, the system was shut down, and the next day the same process was done at 10 LPM. It soon became obvious that as the flow rate decreased, it would take longer for the air to reach its maximum temperature. At 15 LPM the tests would take 30 minutes, and for the 10 LPM tests the experiments could last as long as 45 minutes.

Once the first 9 tests were complete and the data looked consistent, the pebble-bed heater was unbolted. The 0.635 cm (1/4") ball bearings were then swapped out for the 0.476 cm (3/16”) size. 735 carbon steel balls were required to fill the chamber this time. Then, the system was re-assembled to prepare for the next round of testing. The voltage-current relationship for the 0.476 cm (3/16”) spheres was the linear relationship shown in equation 5 and figure 45 within 0.05 amps.

$$\mathrm{I\ [A]} = 0.3959 \left[\frac{\mathrm{A}}{\mathrm{V}}\right] * \mathrm{V\ [V]} \qquad \text{Eq. 5}$$

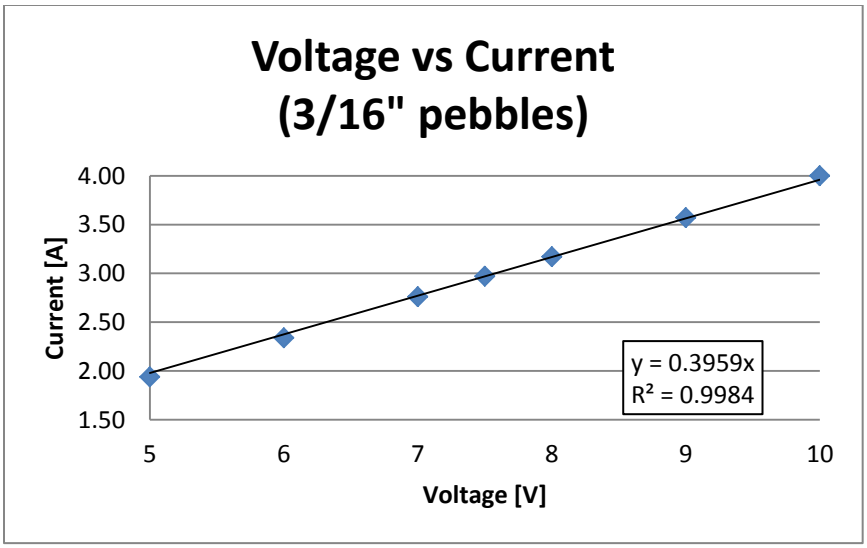

Figure 45. Voltage-current relationship for 0.476 cm (3/16”) balls.

With the 0.476 cm (3/16”) pebbles, testing was conducted in the same manner as with the 0.635 cm (1/4”) pebbles. The 20 LPM test set was performed first for each of the three power levels, the three 15 LPM tests the following day, and the final set at 10 LPM the day after that.

Once the second set of 9 tests had been run and produced reasonable results, the 0.476 cm (3/16”) spheres were changed out for the smaller 0.318 cm (1/8”) size. 2,500 of these balls were needed to fill the center section. Once the pebble-bed heater was re-constructed, the new current-voltage relationship was found to be equation 6 from figure 46.

$$\mathrm{I\ [A]} = 0.3342 \left[\frac{\mathrm{A}}{\mathrm{V}}\right] * \mathrm{V\ [V]} \qquad \text{Eq. 6}$$

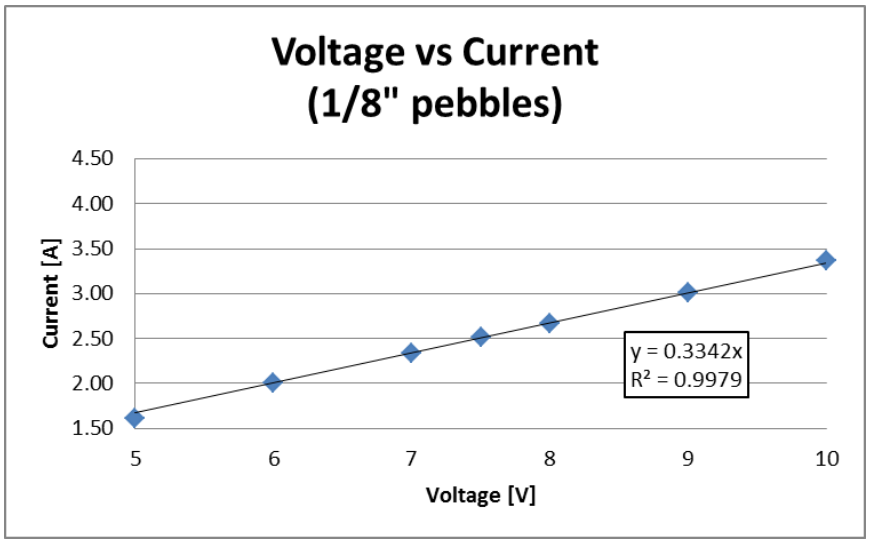

Figure 46. Voltage-current relationship for 0.0.318 cm (1/8”) balls.

The same testing procedure was followed for this group of 9 tests as the 0.635 cm (1/4”) and 0.476 cm (3/16”) experiments. After three more days, the remaining 9 data sets of temperature and pressure values were recorded, and then all 27 tests had been completed. Now that all testing had concluded, the data could be observed and analyzed to search for the behavior of a pebble-bed heater powered by magnetic induction and for a relationship between the Dimensionless Heat Transfer, Dimensionless Power, and Reynolds number.

CHAPTER 5

RESULTS

The experiment data from each of the 27 tests was recorded in an organized and easy to read table (Table 1). The table shows how the maximum temperature would increase and decrease under the different variable combinations. The pebble-bed heater hardly had an effect on the pressure with the largest pressure increase being less than 650 Pa (0.1 psi); therefore, pressure will be left out of this analysis and considered to be constant.

Pebble D	Flow Rate	Current	Voltage	Power	$Temp_{in}$	$Temp_{out}$	$Temp_{in}$	$Temp_{out}$	$Temp_{in}$	$Temp_{out}$	ΔT	ΔT
[in]	[LPM]	[A]	[V]	[W]	[F]	[F]	[C]	[C]	[K]	[K]	[F]	[K]
1/8	20	3.34	10	33.4	75.7	162.4	24.3	72.4	297.4	345.6	86.7	48.2
1/8	20	2.49	7.5	18.7	74.4	120.8	23.6	49.3	296.7	322.5	46.4	25.8
1/8	20	1.64	5	8.2	73.0	93.2	22.8	34.0	295.9	307.2	20.2	11.2
1/8	15	3.34	10	33.4	76.8	182.7	24.9	83.7	298.0	356.9	105.9	58.8
1/8	15	2.49	7.5	18.7	76.6	137.6	24.8	58.7	297.9	331.8	61.0	33.9
1/8	15	1.64	5	8.2	76.8	102.6	24.9	39.2	298.0	312.4	25.8	14.3
1/8	10	3.34	10	33.4	74.7	203.4	23.7	95.2	296.9	368.4	128.7	71.5
1/8	10	2.49	7.5	18.7	73.6	148.2	23.1	64.6	296.3	337.7	74.6	41.4
1/8	10	1.64	5	8.2	73.5	105.5	23.1	40.8	296.2	314.0	32.0	17.8
3/16	20	3.99	10	39.9	73.8	166.4	23.2	74.7	296.4	347.8	92.6	51.4
3/16	20	2.96	7.5	22.2	72.9	124.5	22.7	51.4	295.9	324.5	51.6	28.7
3/16	20	1.94	5	9.7	72.5	96.4	22.5	35.8	295.7	308.9	23.9	13.3
3/16	15	3.99	10	39.9	72.8	189.2	22.7	87.3	295.8	360.5	116.4	64.7
3/16	15	2.96	7.5	22.2	72.5	139.6	22.5	59.8	295.7	332.9	67.1	37.3
3/16	15	1.94	5	9.7	72.1	105.8	22.3	41.0	295.4	314.2	33.7	18.7
3/16	10	3.99	10	39.9	75.6	214.1	24.2	101.2	297.4	374.3	138.5	76.9
3/16	10	2.96	7.5	22.2	75.6	160.4	24.2	71.3	297.4	344.5	84.8	47.1
3/16	10	1.94	5	9.7	75.6	115.6	24.2	46.4	297.4	319.6	40.0	22.2
1/4	20	4.43	10	44.3	73.4	188.7	23.0	87.1	296.2	360.2	115.3	64.1
1/4	20	3.28	7.5	24.6	72.8	140.2	22.7	60.1	295.8	333.3	67.4	37.4
1/4	20	2.14	5	10.7	72.4	107.2	22.4	41.8	295.6	314.9	34.8	19.3
1/4	15	4.43	10	44.3	73.2	212.2	22.9	100.1	296.0	373.3	139.0	77.2
1/4	15	3.28	7.5	24.6	72.7	157.5	22.6	69.7	295.8	342.9	84.8	47.1
1/4	15	2.14	5	10.7	72.2	117.2	22.3	47.3	295.5	320.5	45.0	25.0
1/4	10	4.43	10	44.3	73.2	233.0	22.9	111.7	296.0	384.8	159.8	88.8
1/4	10	3.28	7.5	24.6	72.8	176.3	22.7	80.2	295.8	353.3	103.5	57.5
1/4	10	2.14	5	10.7	72.3	132.1	22.4	55.6	295.5	328.8	59.8	33.2

Table 1. Temperature data from all 27 tests in °F, °C, and K.

In short, the exit temperature would increase if the voltage/power applied to the system increased as seen in figures 47-49, since a greater current would be induced, and the magnetic field would be stronger. The error bars were not included in the plots, since the uncertainty was

only +/- 0.1571 K (+/- 0.2828 °F). Except for the 10 LPM test with the 0.635 cm (1/4”) ball bearings, the trendline equations are more than 96% accurate.

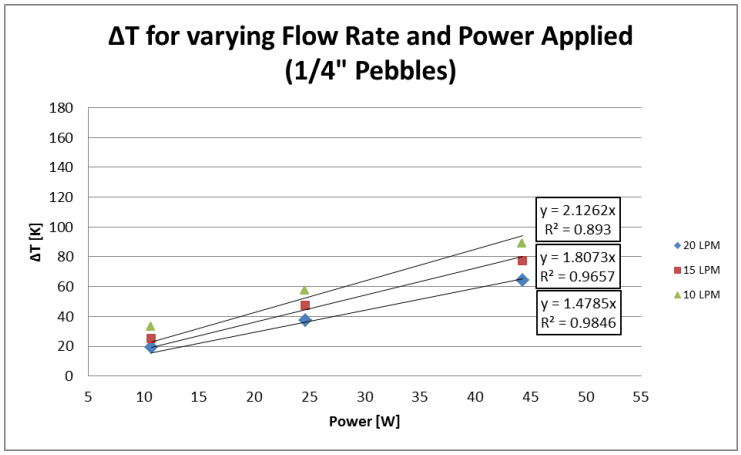

Figure 47. Temperature change vs power supplied at fixed flow rate for 0.635 cm (1/4") balls.

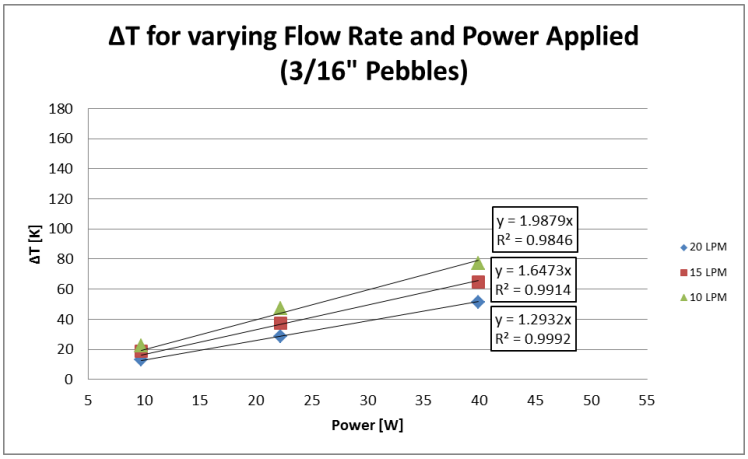

Figure 48. Temperature change vs power supplied at fixed flow rate for 0.476 cm (3/16") balls.

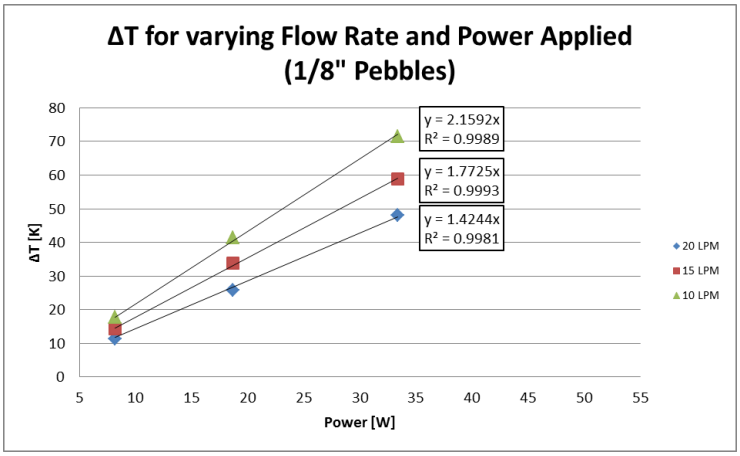

Figure 49. Temperature change vs power supplied at fixed flow rate for 0.318 cm (1/8") balls.

If the flow rate decreased, the exit temperature would also increase. The faster moving air would cool the spheres and not allow them to reach as high of a temperature. As mentioned earlier, if the flow rate decreased, it would take longer for the temperature to stagnate. Therefore, there is a downside to lowering the flow rate to increase the temperature if time is a factor. Lastly, the exit temperature increased as the diameter of the ball bearings increased. This was due to the fact that the larger diameter balls had a lower overall volume and surface area compared to the smaller sizes (Table 2). If the same amount of current is being induced on a smaller total surface area, then there will be more resistance and more heat generated. Likewise, an identical alternating magnetic field being applied to smaller volume of metal will produce a greater hysteresis loss effect.

Number of Carbon Steel Balls			Volume of Carbon Steel Balls			Surface Area of Carbon Steel Balls			Mass of Carbon Steel Balls		
#_1/4	300	--	V_1/4	2.454	in^3	SA_1/4	58.90	in^2	m_1/4	0.69704087	lb_m
#_3/16	735	--	V_3/16	2.537	in^3	SA_3/16	81.18	in^2	m_3/16	0.72045709	lb_m
#_1/8	2500	--	V_1/8	2.557	in^3	SA_1/8	122.72	in^2	m_1/8	0.72608424	lb_m
#_1/4	300	--	Vol_1/4	4.02E-05	m^3	SA_1/4	3.80E-02	m^2	m_1/4	3.16E-01	kg
#_3/16	735	--	Vol_3/16	4.16E-05	m^3	SA_3/16	5.24E-02	m^2	m_3/16	3.26E-01	kg
#_1/8	2500	--	Vol_1/8	4.19E-05	m^3	SA_1/8	7.92E-02	m^2	m_1/8	3.29E-01	kg

Table 2. Volume, surface area, and mass for the different ball sizes in imperial and metric units.

In order to convert the results into dimensionless form, several air properties had to be found first: density, specific heat, thermal conductivity, and kinematic viscosity. Since each property was dependent on temperature, the same value could not be used for every test. The temperature used to determine the exact density, specific heat, conductivity, or viscosity was the exit temperature of the air for each test [16,17,18]. The temperature dependent value for each property was linearly interpolated from the appropriate table. The density range was 0.923 to 1.18 kg/m^3; specific heat was 1005 to 1011 J/kg-K; conductivity was 0.0267 to 0.0322 W/m-K; and kinematic viscosity was $1.64*10^{-5}$ to $2.43*10^{-5}$ m^2/s. In addition to the air properties, the thermal conductivity of carbon steel was also needed and found to be 43 W/m-K [20].

With the air density known from the table, the mass flow rate could be calculated from the volumetric flow rate using equation 7. Then, the amount of heat given to the air via convection (Q_{conv}) was able to be determined using equation 8 [33]. Finally, the efficiency of the system could be found for each case using equation 9.

$$\dot{m}\left[\frac{kg}{s}\right] = \dot{V}\left[\frac{m^3}{s}\right]\rho\left[\frac{kg}{m^3}\right] \quad \text{Eq. 7}$$

$$Q_{conv}[W] = \dot{m}\left[\frac{kg}{s}\right]c_p\left[\frac{J}{kgK}\right](T_{out} - T_{in})[K] \quad \text{Eq. 8}$$

$$\text{Efficiency}\,[\%] = \frac{Q_{conv}[W]}{P[W]} * 100 \quad \text{Eq. 9}$$

The greatest efficiency was 67.8% using the 0.635 cm (1/4") balls, 20 LPM, and 10.7 watts; the lowest efficiency was 30.7% with 0.476 cm (3/16") balls, 10 LPM, and 39.9 watts. The efficiency would typically increase at higher flow rates and lower power as seen in figure 50. The pebble size did not have a consistent effect on the efficiency, so only one plot was included. Error bars were not included in this plot, since the efficiency error was between +/-

0.01 and +/- 0.03. The power lost in the system could be heat conducted through the wall of the pebble chamber as well as the inefficiencies in the heat generation process from the induction heater.

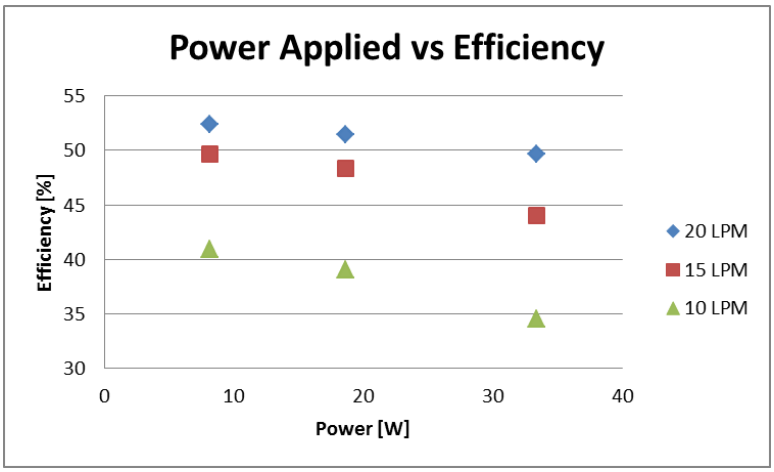

Figure 50. Power applied through the solenoid vs heating efficiency with 0.476 cm (3/16") balls.

To determine the Dimensionless Heat Transfer, the heat generated in the steel balls via conduction had to be calculated. The first step was to find the "resistance" of air and the "resistance" of steel to conduction. The resistance of air and steel required a characteristic length (L_c) to be chosen for each. For this experiment, the characteristic length of air in the pebble chamber would be the cube root of the volume of air as shown in equation 10. Likewise, the characteristic length of steel would be the cube root of the volume of steel inside the chamber (Equation 11).

$$L_{c_{air}}[m] = \sqrt[3]{V_{pipe}[m^3] - V_{steel}[m^3]} \quad \text{Eq. 10}$$

$$L_{c_{steel}}[m] = \sqrt[3]{V_{steel}[m^3]} \quad \text{Eq. 11}$$

The cross-section of both air and steel was assumed to be a solid circle, so the "effective area" of each would just be the area of a circle with the characteristic length being the diameter

(Equations 12 and 13). Once the effective areas were determined, the resistances could finally be calculated using equations 14 and 15 with the thermal conductivity (k) values found in the tables earlier [33].

$$A_{air}[m^2] = \frac{\pi(L_{c_{air}}[m])^2}{4} \quad \text{Eq. 12}$$

$$A_{steel}[m^2] = \frac{\pi(L_{c_{steel}}[m])^2}{4} \quad \text{Eq. 13}$$

$$R_{air}\left[\frac{K}{W}\right] = \frac{L_{c_{air}}[m]}{k_{air}\left[\frac{W}{mK}\right]A_{air}[m^2]} \quad \text{Eq. 14}$$

$$R_{steel}\left[\frac{K}{W}\right] = \frac{L_{c_{steel}}[m]}{k_{steel}\left[\frac{W}{mK}\right]A_{steel}[m^2]} \quad \text{Eq. 15}$$

The resistances would be treated as though they were acting in parallel (Figure 51), since the air and pebbles are mixed together in the same pipe section. With this in mind, the heat in the spheres via conduction can be calculated with equation 16, and then the Dimensionless Heat Transfer (N_{HT}) can finally be determined from equation 17 [33].

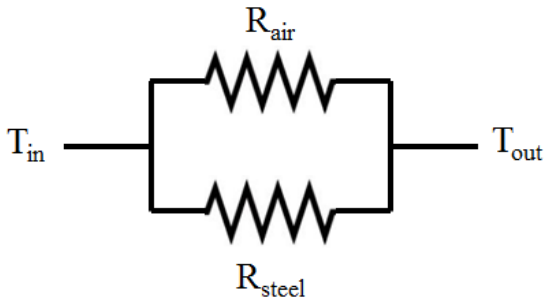

Figure 51. Resistance diagram for air and steel.

$$Q_{cond}[W] = \frac{(T_{out} - T_{in})[K]}{\left(\frac{1}{R_{air}}\left[\frac{W}{K}\right] + \frac{1}{R_{steel}}\left[\frac{W}{K}\right]\right)^{-1}} \quad \text{Eq. 16}$$

$$N_{HT} = \frac{Q_{conv}[W]}{Q_{cond}[W]} \quad \text{Eq. 17}$$

The second dimensionless number in this experiment would be the Reynolds number. The kinematic viscosity (ν) values were found already by linearly interpolating the data tables, and the characteristic length of air has been calculated, so the only unknown in the equation was the air's velocity. The velocity could easily be determined by dividing the volumetric flow rate by the air's effective area as seen in equation 18. The Reynolds number (Re) was then calculated using equation 19 [33].

$$U\left[\frac{m}{s}\right] = \frac{\dot{V}\left[\frac{m^3}{s}\right]}{A_{air}[m^2]} \quad \text{Eq. 18}$$

$$Re = \frac{U\left[\frac{m}{s}\right] L_{c_{air}}[m]}{\nu\left[\frac{m^2}{s}\right]} \quad \text{Eq. 19}$$

The final dimensionless number would account for power and be called "N_P." The only unknown in equation 20 was the operating frequency. An oscilloscope lead was attached to either end of the solenoid coil and the frequency of the sine wave was measured to be 21,740 Hz as seen in figure 52. The frequency was unaffected by the power level; an increase or decrease in power would only change the amplitude of the wave. The Dimensionless Power could now be found.

$$N_P = \frac{P[W]}{\left(\omega\left[\frac{1}{s}\right]\right)^3 m_{balls}[kg] SA_{balls}[m^2]} \quad \text{Eq. 20}$$

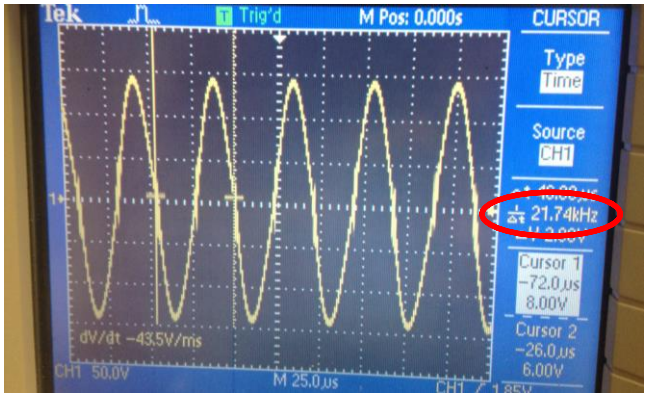

Figure 52. Sine wave and frequency of the experiment.

Once all three dimensionless numbers had been calculated for each case, a linear relationship was found between the three variables using equation 21. The results were then plotted against each other as shown in figure 53. Error bars were included, and most cases overlap with the linear trendline. Values for the uncertainty can be found in the Appendix. The Dimensionless Heat Transfer and Reynolds number would both increase as flow rate increased, power decreased, and pebble diameter decreased. This chart can be used by other researchers to compare and verify the data from their own magnetic induction pebble-bed heater as well as predict the output of a pebble-bed heater. All values for calculating the dimensionless numbers can be seen in tables 3 through 5. A further discussion of the results will be covered in the following section.

$$N_{HT} = (N_P)^{\frac{1}{6}}(0.098081\mathrm{Re} - 0.222209) \qquad \text{Eq. 21}$$

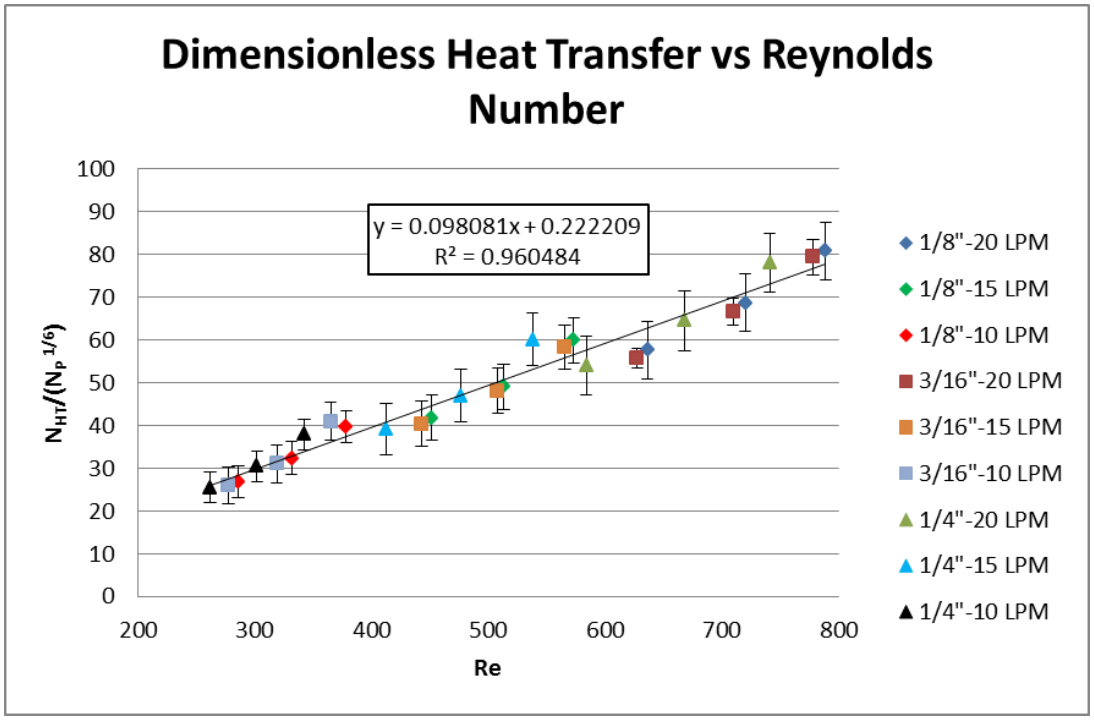

Figure 53. Dimensionless relationship in a magnetic induction pebble-bed heater.

Pebble D	Flow Rate	Flow Rate	Flow Rate	Current	Voltage	Power	ρ_{air}	Mass Flow	c_p	Q_{conv}	Efficiency
[in]	[LPM]	[GPM]	[m^3/s]	[A]	[V]	[W]	[kg/m^3]	[kg/s]	[J/kg-K]	[W]	[%]
1/8	20	5.28	3.33E-04	3.34	10	33.4	1.023	3.41E-04	1009	16.6	49.6
1/8	20	5.28	3.33E-04	2.49	7.5	18.7	1.109	3.70E-04	1007	9.6	51.4
1/8	20	5.28	3.33E-04	1.64	5	8.2	1.140	3.80E-04	1005	4.3	52.4
1/8	15	3.96	2.50E-04	3.34	10	33.4	0.990	2.48E-04	1009	14.7	44.0
1/8	15	3.96	2.50E-04	2.49	7.5	18.7	1.055	2.64E-04	1009	9.0	48.4
1/8	15	3.96	2.50E-04	1.64	5	8.2	1.127	2.82E-04	1005	4.1	49.6
1/8	10	2.64	1.67E-04	3.34	10	33.4	0.958	1.60E-04	1009	11.5	34.5
1/8	10	2.64	1.67E-04	2.49	7.5	18.7	1.045	1.74E-04	1009	7.3	39.0
1/8	10	2.64	1.67E-04	1.64	5	8.2	1.124	1.87E-04	1005	3.3	40.9
3/16	20	5.28	3.33E-04	3.99	10	39.9	1.015	3.38E-04	1008	17.5	43.9
3/16	20	5.28	3.33E-04	2.96	7.5	22.2	1.102	3.67E-04	1007	10.6	47.7
3/16	20	5.28	3.33E-04	1.94	5	9.7	1.145	3.82E-04	1005	5.1	52.6
3/16	15	3.96	2.50E-04	3.99	10	39.9	0.980	2.45E-04	1009	16.0	40.0
3/16	15	3.96	2.50E-04	2.96	7.5	22.2	1.060	2.65E-04	1009	10.0	44.8
3/16	15	3.96	2.50E-04	1.94	5	9.7	1.123	2.81E-04	1005	5.3	54.6
3/16	10	2.64	1.67E-04	3.99	10	39.9	0.946	1.58E-04	1009	12.2	30.7
3/16	10	2.64	1.67E-04	2.96	7.5	22.2	1.025	1.71E-04	1009	8.1	36.5
3/16	10	2.64	1.67E-04	1.94	5	9.7	1.180	1.97E-04	1006	4.4	45.4
1/4	20	5.28	3.33E-04	4.43	10	44.3	0.980	3.27E-04	1009	21.1	47.7
1/4	20	5.28	3.33E-04	3.28	7.5	24.6	1.060	3.53E-04	1009	13.3	54.2
1/4	20	5.28	3.33E-04	2.14	5	10.7	1.120	3.73E-04	1005	7.3	67.8
1/4	15	3.96	2.50E-04	4.43	10	44.3	0.946	2.37E-04	1009	18.4	41.6
1/4	15	3.96	2.50E-04	3.28	7.5	24.6	1.029	2.57E-04	1009	12.2	49.6
1/4	15	3.96	2.50E-04	2.14	5	10.7	1.150	2.88E-04	1006	7.2	67.6
1/4	10	2.64	1.67E-04	4.43	10	44.3	0.923	1.54E-04	1011	13.8	31.2
1/4	10	2.64	1.67E-04	3.28	7.5	24.6	1.000	1.67E-04	1009	9.7	39.2
1/4	10	2.64	1.67E-04	2.14	5	10.7	1.085	1.81E-04	1008	6.1	56.6

Table 3. Efficiency and Heat Transfer data.

k_{air}	L_{c_air}	A_{eff_air}	R_{air}	L_{c_steel}	A_{eff_steel}	R_{steel}	Q_{cond}	N_{HT}
[W/m-K]	[m]	[m^2]	K/W	[m]	[m^2]	K/W	[W]	[--]
0.0294	0.03281	8.456E-04	6.128E+03	3.473E-02	9.474E-04	3.741E+00	1.288E+01	1.286
0.0278	0.03281	8.456E-04	6.490E+03	3.473E-02	9.474E-04	3.741E+00	6.895E+00	1.392
0.0267	0.03281	8.456E-04	6.754E+03	3.473E-02	9.474E-04	3.741E+00	3.002E+00	1.428
0.0302	0.03281	8.456E-04	5.966E+03	3.473E-02	9.474E-04	3.741E+00	1.574E+01	0.934
0.0284	0.03281	8.456E-04	6.339E+03	3.473E-02	9.474E-04	3.741E+00	9.064E+00	0.995
0.0271	0.03281	8.456E-04	6.661E+03	3.473E-02	9.474E-04	3.741E+00	3.834E+00	1.059
0.0310	0.03281	8.456E-04	5.809E+03	3.473E-02	9.474E-04	3.741E+00	1.913E+01	0.602
0.0289	0.03281	8.456E-04	6.247E+03	3.473E-02	9.474E-04	3.741E+00	1.109E+01	0.657
0.0272	0.03281	8.456E-04	6.633E+03	3.473E-02	9.474E-04	3.741E+00	4.755E+00	0.704
0.0296	0.03291	8.508E-04	6.058E+03	3.464E-02	9.425E-04	3.760E+00	1.369E+01	1.282
0.0279	0.03291	8.508E-04	6.416E+03	3.464E-02	9.425E-04	3.760E+00	7.628E+00	1.390
0.0268	0.03291	8.508E-04	6.681E+03	3.464E-02	9.425E-04	3.760E+00	3.533E+00	1.442
0.0305	0.03291	8.508E-04	5.880E+03	3.464E-02	9.425E-04	3.760E+00	1.721E+01	0.929
0.0285	0.03291	8.508E-04	6.283E+03	3.464E-02	9.425E-04	3.760E+00	9.919E+00	1.005
0.0272	0.03291	8.508E-04	6.590E+03	3.464E-02	9.425E-04	3.760E+00	4.982E+00	1.060
0.0314	0.03291	8.508E-04	5.696E+03	3.464E-02	9.425E-04	3.760E+00	2.048E+01	0.598
0.0293	0.03291	8.508E-04	6.107E+03	3.464E-02	9.425E-04	3.760E+00	1.254E+01	0.648
0.0276	0.03291	8.508E-04	6.498E+03	3.464E-02	9.425E-04	3.760E+00	5.913E+00	0.744
0.0304	0.03332	8.721E-04	5.739E+03	3.426E-02	9.220E-04	3.844E+00	1.667E+01	1.266
0.0285	0.03332	8.721E-04	6.124E+03	3.426E-02	9.220E-04	3.844E+00	9.747E+00	1.370
0.0272	0.03332	8.721E-04	6.416E+03	3.426E-02	9.220E-04	3.844E+00	5.032E+00	1.441
0.0314	0.03332	8.721E-04	5.570E+03	3.426E-02	9.220E-04	3.844E+00	2.010E+01	0.917
0.0292	0.03332	8.721E-04	5.981E+03	3.426E-02	9.220E-04	3.844E+00	1.226E+01	0.997
0.0276	0.03332	8.721E-04	6.324E+03	3.426E-02	9.220E-04	3.844E+00	6.507E+00	1.111
0.0322	0.03332	8.721E-04	5.428E+03	3.426E-02	9.220E-04	3.844E+00	2.311E+01	0.597
0.0300	0.03332	8.721E-04	5.833E+03	3.426E-02	9.220E-04	3.844E+00	1.497E+01	0.646
0.0282	0.03332	8.721E-04	6.193E+03	3.426E-02	9.220E-04	3.844E+00	8.648E+00	0.700

Table 4. Additional Heat Transfer data.

Velocity [m/s]	Viscosity [m^2/s]	Reynolds # [--]	N_P [--]	$N_{HT}/(N_P^{1/6})$ [--]
3.94E-01	2.03E-05	636	1.248E-10	57.55
3.94E-01	1.80E-05	720	6.972E-11	68.60
3.94E-01	1.64E-05	789	3.057E-11	80.75
2.96E-01	2.15E-05	452	1.248E-10	41.77
2.96E-01	1.89E-05	513	6.972E-11	49.04
2.96E-01	1.69E-05	573	3.057E-11	59.87
1.97E-01	2.27E-05	285	1.248E-10	26.94
1.97E-01	1.95E-05	331	6.972E-11	32.39
1.97E-01	1.71E-05	378	3.057E-11	39.81
3.92E-01	2.06E-05	627	1.492E-10	55.65
3.92E-01	1.82E-05	709	8.309E-11	66.55
3.92E-01	1.66E-05	778	3.617E-11	79.27
2.94E-01	2.19E-05	443	1.492E-10	40.34
2.94E-01	1.90E-05	508	8.309E-11	48.10
2.94E-01	1.71E-05	565	3.617E-11	58.31
1.96E-01	2.33E-05	277	1.492E-10	25.96
1.96E-01	2.02E-05	319	8.309E-11	31.01
1.96E-01	1.77E-05	365	3.617E-11	40.89
3.82E-01	2.18E-05	584	1.656E-10	54.03
3.82E-01	1.91E-05	668	9.207E-11	64.45
3.82E-01	1.72E-05	741	3.997E-11	77.96
2.87E-01	2.32E-05	412	1.656E-10	39.12
2.87E-01	2.01E-05	476	9.207E-11	46.93
2.87E-01	1.78E-05	538	3.997E-11	60.09
1.91E-01	2.43E-05	262	1.656E-10	25.49
1.91E-01	2.11E-05	302	9.207E-11	30.39
1.91E-01	1.86E-05	342	3.997E-11	37.87

Table 5. Reynolds number and Dimensionless Power data.

After the efficiency and dimensionless analyses were completed, a study of the inefficiencies and uncertainty was performed. At 100% efficiency, the power supplied to the system would equal the power converted to heating the air. However, the efficiency for this system was always between 30% and 70%, meaning that some heat was lost through the pipe wall or by some other means.

The heat lost through the pipe wall was not consistent along the pipe. More heat would escape towards the pipe's exit than inlet, since the air's temperature would increase as it went through the heating chamber. Regardless, to account for maximum loss, the outer wall temperature of the pipe was assumed to be uniform, and the value used would be the temperature at the exit of the pipe. Using one of the T-type thermocouples from the experiment, the outer wall temperature was measured just below the top flange once the exit air temperature had

leveled off. With these temperature readings, the amount of heat lost through the wall could be calculated using equation 23 [33]. The amount of power that did not go to heating the air or escaping through the wall was called $Q_{remaining}$ and calculated with equation 24.

$$Q_{loss\_wall}[W] = \frac{2\pi k_{plastic}\left[\frac{W}{mK}\right] L_{wall}[m](T_{out} - T_{wall})[K]}{\ln\left(\frac{r_{out}[m]}{r_{in}[m]}\right)} \quad \text{Eq. 23}$$

$$Q_{remaining}[W] = P[W] - Q_{conv}[W] - Q_{loss\_wall}[W] \quad \text{Eq. 24}$$

The amount of power remaining ranged from 9.63 watts to negative 3.44 watts as seen in table 6, but in an ideal case it should be zero watts. There were three negative values greater than 1 watt for $Q_{remaining}$, and each of them occurred at 5 volts. Either the quantity of heat escaping through the pipe was too high or the heat to convection was too low. The opposite could be said for the readings producing positive values greater than 1 watt. The inaccuracy in the amount of $Q_{remaining}$ could be due to the fact that heat lost through the pipe was assumed to be uniform. There could also be other sources of power loss in the induction heater system that were not accounted for. The uncertainty of the power supplied, the heat to convection, and the heat lost through the pipe were calculated and can be seen in table 6 along with the rest of the data from this analysis. The calculated uncertainty was able to account for a few of the experiments, but most fell outside of the range. Therefore, the uncertainty analysis does not completely account for all error. A more in depth study into the losses of the induction heater system and the temperature loss across the pipe would need to be conducted.

Pebble D	Flow Rate	Power	Q_{conv}	T_{outer_wall}	T_{outer_wall}	Q_{loss_wall}	$Q_{remaining}$	U_Power	U_Q_conv+loss	Overlap
[in]	[LPM]	[W]	[W]	[F]	[K]	[W]	[W]	[W]	[W]	[--]
1/8	20	33.4	16.6	121.8	323.0	12.20	4.61	0.500	0.426	No
1/8	20	18.7	9.6	99.1	310.4	6.53	2.52	0.375	0.261	No
1/8	20	8.2	4.3	84.0	302.0	2.77	1.12	0.250	0.149	No
1/8	15	33.4	14.7	132.9	329.2	14.97	3.72	0.500	0.499	No
1/8	15	18.7	9.0	108.3	315.5	8.82	0.81	0.375	0.315	Yes
1/8	15	8.2	4.1	89.1	304.9	4.05	0.07	0.250	0.166	Yes
1/8	10	33.4	11.5	144.2	335.5	17.79	4.07	0.500	0.583	No
1/8	10	18.7	7.3	114.1	318.7	10.27	1.10	0.375	0.375	No
1/8	10	8.2	3.3	90.7	305.8	4.45	0.38	0.250	0.190	Yes
3/16	20	39.9	17.5	124.0	324.3	12.75	9.63	0.500	0.450	No
3/16	20	22.2	10.6	101.1	311.5	7.04	4.59	0.375	0.284	No
3/16	20	9.7	5.1	85.7	303.0	3.21	1.38	0.250	0.165	No
3/16	15	39.9	16.0	136.5	331.2	15.85	8.09	0.500	0.541	No
3/16	15	22.2	10.0	109.3	316.1	9.10	3.17	0.375	0.346	No
3/16	15	9.7	5.3	90.9	305.9	4.49	-0.09	0.250	0.201	Yes
3/16	10	39.9	12.2	150.1	338.8	19.25	8.44	0.500	0.618	No
3/16	10	22.2	8.1	120.7	322.4	11.93	2.18	0.375	0.416	No
3/16	10	9.7	4.4	96.2	308.8	5.83	-0.54	0.250	0.238	No
1/4	20	44.3	21.1	136.2	331.0	15.79	7.40	0.500	0.537	No
1/4	20	24.6	13.3	109.7	316.3	9.18	2.11	0.375	0.349	No
1/4	20	10.7	7.3	91.6	306.3	4.68	-1.24	0.250	0.209	No
1/4	15	44.3	18.4	149.1	338.2	18.99	6.88	0.500	0.621	No
1/4	15	24.6	12.2	119.1	321.6	11.53	0.87	0.375	0.418	No
1/4	15	10.7	7.2	97.1	309.3	6.04	-2.58	0.250	0.260	No
1/4	10	44.3	13.8	160.4	344.5	21.82	8.68	0.500	0.696	No
1/4	10	24.6	9.7	129.4	327.3	14.10	0.87	0.375	0.491	Yes
1/4	10	10.7	6.1	105.2	313.8	8.07	-3.44	0.250	0.316	No

Table 6. Inefficiency data from all 27 experiments.

CHAPTER 6

DISCUSSION

This study was able to research the capabilities and limitations of a magnetic induction pebble-bed heater, design and construct a fully-functional scaled-down model, and determine a pebble-bed heater's behavior under different conditions. The following will be a discussion of the research, experimental findings, potential improvements to the design, and future testing possibilities.

The research in this study determined that if a pebble-bed heater was powered by magnetic induction, it could only be a suitable nuclear reactor simulator for testing nuclear thermal rocket engines if a metal was found that had a melting temperature well above 1,922 K (3,000 °F) and was both magnetic and electrically conductive. However, if the pebble matrix is heated by convection in the same manner as Glenn Research Center's pebble-bed heater had been in the mid 1960's, it is possible to use it as a simulator, and high melting temperature ceramics could be used in the pebble bed instead of steel. The downside to the convection method is that it is limited to at most a 30 second test window before the pebble matrix has cooled too much. This was the reason for looking into magnetic induction as a heat source, since magnetic induction provides a continuous supply of heat, allowing tests to be run for as long as necessary.

For the nuclear simulator case where a magnetic induction pebble-bed heater will actually be used as a nuclear reactor simulator, several important characteristics should be considered when choosing the steel type and grade that will make up the pebble matrix and chamber. First, the steel must be hydrogen-embrittlement-free, since the propellant that will be used for the nuclear rocket engines is hydrogen. Hydrogen embrittlement is a destructive process that makes

high strength steels brittle and eventually fracture after exposure to high temperature hydrogen [4]. At high temperatures, hydrogen atoms can actually seep into certain metals. If several hydrogen atoms gather together in a small pocket inside the metal and form molecules, then the molecules can begin to create internal pressure and eventually cause the metal to crack open [4]. Embrittlement is most commonly found in high strength and low alloy steels, so these should be avoided. It would be a disaster if the chamber cracked, and fractured steel balls could skew results.

Secondly, the metal for the spheres must be magnetic and have a very high melting temperature, as it will obviously be operating at several thousand degrees Kelvin. Melting temperatures for stainless steels range from 1,672 K to 1,803 K (2,550 °F to 2,785 °F), and carbon steels range from 1,683 K to 1,811 K (2,570 °F to 2,800 °F) [10,19]. Even though certain high carbon steels can sustain a slightly greater temperature than the stainless steels, they are not as corrosive resistant or embrittlement-free as some of the stainless steels. It is therefore recommended to choose stainless steel over carbon steel in the nuclear simulator tests. The two stainless steel grades with the highest melting temperature are grades 409 and 410 [10]. Grade 409 is a ferritic stainless steel and subsequently prone to hydrogen embrittlement. Grade 409 is therefore not an option for nuclear testing [8]. However, grade 410 is a martensic stainless steel, which makes it hydrogen-embrittlement-free and magnetic [8]. In conclusion, grade 410 stainless steel is the best candidate for the steel pebbles inside the pebble matrix for the nuclear reactor simulator. If a hydrogen-embrittlement-free steel is later manufactured with a higher melting temperature, then it would clearly be a more suitable option.

In addition to the melting temperature, another setback to the magnetic induction method is the Curie temperature of steel. The Curie temperature is the point at which a material is no

longer magnetic and for most steels this is usually around 1,033 K (1,400 °F). To be a simulator, the heater would need to heat hydrogen up to 1,922 K (3,000 °F). Beyond the Curie temperature, heating is still possible with induction heating but without the hysteresis loss portion of the heat generation. The process would be much slower past this point and require additional power, since only the skin effect would be heating the steel.

A magnetic induction pebble-bed heater still has other beneficial uses besides a nuclear reactor simulator, especially at lower temperature levels. Due to its high efficiency, no moving parts, and non-invasive, flameless method of heating gases and fluids, there are many possible applications for the heater. The device was found to have been used on at least two other experiments. One was to test the cooling capabilities of salt by putting a specialized salt in a tube full of graphite spheres and heating the graphite with an induction heater. Another experiment was to test the cooling abilities of a metal tube packed with little balls inside that has air flowing through it compared to a solid metal pipe with air flowing over it. It could also be used in a home as a local hot water heater for a sink/shower or any instance where a gas, liquid, or even a metal object inside a tube needed to be heated without a flame or any invasive tactics.

The design of the experiment allowed all 27 tests to be run and data to be recorded. The better aspects of the pebble-bed heater design from this experiment include the two middle copper spacers and the bronze wool. The copper spacers allowed the temperature and pressure measuring instruments access to the air flow directly before and after the heating process without allowing any air to leak out. The bronze wool successfully normalized the flow of the air, so that it had a uniform distribution when it met the two sets of instruments and when it entered the pebble matrix.

The pebble-bed heater design had several flaws. The main issues being insulation and weight. In order to hopefully solve the insulation issue in the future, the center section of the pebble-bed heater should be made out of a high melting temperature ceramic. Since aluminum, brass, and copper are all conductive, none of them are suitable candidates. Conductive metals would not only be affected by the skin effect but would also risk shorting out the system if any contact is made with the work coil of the induction heater. While 3D printed ABS plastic was a great substitute for this low temperature test environment, it would not be feasible for most applications given its low "melting" temperature. Therefore, a ceramic with a high melting temperature should be used as the material for the pebble chamber and be molded or 3D printed into the appropriate flange-pipe-flange shape for the job at hand. The chamber could also be wrapped or coated in additional insulation to reduce heat lost through conduction in the pipe wall and improve the overall efficiency.

There was another insulation issue with the upstream thermocouple and the differential pressure transducer (DPT). The induced current from the work coil would interfere with the DPT and first thermocouple's readings, so all pressure and intake temperature readings were recorded once the maximum temperature was reached and just after the induction heater was turned off. The exit temperature and volumetric flow rate would be the same but without the electrical interference. To resolve this issue, there should be a rubber or non-conductive thin layer between the instrument spacers and the center section. In addition, the metal mesh circles could be attached to the rubber washer instead of cardboard. To insulate the DPT, it should be placed on top of a piece of wood, cardboard, plastic, or other non-conductive material. These adjustments were not performed in this set of experiments but will hopefully reduce the amount of interference from induced currents in the future.

The second major issue with the design was the weight of the pebble-bed heater. Copper was chosen as the material for most of the heater, since it was not magnetic and easy to machine; however, copper is both heavy and expensive. Copper was the main material used in this experiment, so the system weighed close to 111 N (25 lb). In hind sight, aluminum would be the best option for the disk spacers in the middle and at either end. Copper is 73% heavier than aluminum, so switching to aluminum would eliminate a lot of the weight [57]. The thickness of the end spacers could also be cut in half, and it would still be more than enough for the NPT fittings on either end to screw in. In order to remove all copper, the two smaller flange-pipe-flange sections could be made out of aluminum or the same high melting temperature ceramic as the center pipe section. Aluminum would work for these sections because there is no chance of touching the work coil.

The induction heater schematic chosen was fitting for this application. The heater was easy enough for someone with minimal electrical experience to learn how it worked and put all the pieces together. There were not many components, and the parts were not difficult to find or expensive. Lastly, this circuit was capable of heating metal to almost 533 K (500 °F), which was more than enough for the experiment.

Several improvements that could be made to the induction heater would be the work coil and the addition of a breadboard. The one-piece, 0.847 cm (1/3”), copper pipe originally used in the experiment produced higher temperatures than the 12 gauge insulated wire that was later put in its place. The pipe could also handle higher currents and even be water cooled if the pipe were to get too hot. If the pipe, flanges, and bolts are either non-conductive or insulated from the solenoid, then the copper pipe should be used for the solenoid.

Since the breadboards in the lab were only able to support up to one amp of current, a floating circuit had to be made. However, it is recommended that a breadboard be purchased that could handle 5 amps or maybe even more than 5 amps and used for the induction heater circuit. The resistors, diodes, capacitors, and transistors could then easily be securely connected to the breadboard, power supply, and one another. One of the frequent issues during the testing process was with the wires attached to the transistors. The wires would occasionally be bumped, and the solder would come loose, then the transistors would short circuit instantly and need to be replaced. If the transistors could be plugged straight into a breadboard, then the problem would not be as likely to happen. This would allow for less maintenance and fewer transistors would need to be ordered.

The behavior of the heater was tested over 27 experiments at different conditions. This study shows how the exit temperature is affected by the flow rate, pebble size, and power level. It was found that the amount of temperature change would increase with increasing pebble size, decreasing flow rate, and increasing power. As the flow rate decreased, it would take longer for the test to reach the maximum temperature. This should be taken into account if time is a factor. Changing the amount of power supplied to the system had the quickest effect on the temperature. Therefore, increasing the power is the best way to increase the exit temperature. The overall efficiency would decrease as the power increased and as the flow rate decreased, so a higher exit temperature would mean more wasted power.

After a series of calculations, the Dimensionless Heat Transfer, Dimensionless Power, and Reynolds number were calculated for each of the 27 cases. The results were put into a chart, so that the data can be used to predict the capabilities of a future pebble-bed heater or verify the results of an existing pebble-bed heater. The same characteristic length formula should be used

when verifying and predicting results. A linear trendline was used to establish the relationship between the three dimensionless numbers. If the Reynolds number is held constant, then the Heat Transfer number would increase with an increase in flow rate, a decrease in pebble diameter, and a decrease in power.

In conclusion:

- For a magnetic induction pebble-bed heater to function as a nuclear reactor simulator, a magnetic metal would have to be found with a melting temperature above 1,922 K (3,000 °F) and as high of a Curie temperature as possible.
- The exit temperature through the pebble-bed heater increases with increasing power, decreasing flow rate, and increasing pebble size.
- There is almost no difference in pressure with the small-scale pebble-bed heater.
- The efficiency increases with decreasing power and increasing flow rate.
- If Reynolds number is constant, the Heat Transfer number will increase with decreasing power, increasing flow rate, and decreasing pebble size.

$$N_{HT} = (N_P)^{\frac{1}{6}}(0.098081\mathrm{Re} - 0.222209)$$

Future work:

- Test the properties and relationships of a different gas or even a liquid.
- Do a Prandtl number analysis between different gases.
- Test at different pipe diameters.
- Use a high melting temperature ceramic for the heating chamber.

- Use a small, copper pipe instead of a thick wire for the work coil.
- Put the circuit in a 5 amp or more breadboard
- Electrically insulate the middle instrumentation disks from the heating chamber
- Use more aluminum and less copper for the parts of the experiment (except the work coil)

REFERENCES

[1] Acero, J., et al. "The domestic induction heating appliance: An overview of recent research" *Applied Power Electronics Conference and Exposition, 2008. APEC 2008. Twenty-Third Annual IEEE* (Feb 2008): 651-657. Presented.

[2] Anderson, W. & Heister, S. (2005). *Purdue Propulsion: Rocket Propulsion Short Course Notes.* Purdue University School of Aeronautics and Astronautics. West Lafayette, IN. Print.

[3] ASM International. "Theory of Heating by Induction." *Practical Induction Heat Treating*. 2001. Print.

[4] Barnoush, Afrooz. *Hydrogen Embrittlement*. Tech. 2011. Print. <http://www.uni-saarland.de/fak8/wwm/research/phd_barnoush/hydrogen.pdf>.

[5] Braun, Bobby. "Open Letter to College Students." NASA. Letter. 9 Aug. 2010. <http://www.nasa.gov/offices/oct/home/college_letter_detail.html>.

[6] Burnett, Richie. "High Frequency Induction Heating." Web. 3 Mar. 2013. <http://www.richieburnett.co.uk/indheat.html>.

[7] Corliss, William R., and Francis C. Schwenk. "NERVA Flow Diagram." *Nuclear Propulsion for Space*. NASA, 1971. Web. 21 Jan. 2014.

[8] CSI Equipment and Services. *Stainless Steel Selection Guide - Central States Industrial*, Central States Industrial Equipment and Services Inc., Springfield, MO., 2001. Print. <http://www.csidesigns.com/PDFs/SSSguide.pdf>.

[9] Davenne, Tristan, Otto Caretta, and Peter Loveridge. *A Static Packed Bed Target*. Presentation. 2011.

[10] Davis, Joseph R. *ASM Specialty Handbook Stainless Steels*. ASM International, 1995. Print.

[11] Digikey. "1N4007-E3/54GICT-ND: Schottky Rectifier Diode, 1 A, 1 kV." Web. 20 Apr. 2013. <http://www.digikey.com/product-detail/en/1N4007-E3%2F54/1N4007-E3%2F54GICT-ND/868990>.

[12] Digikey. "497-7520-5-ND: MOSFET Transistor, N-Channel, 100 V, 35 A." Web. 22 Apr. 2013. <http://www.digikey.com/product-search/en?lang=en&site=us&KeyWords=497-7520-5-nd&x=0&y=0>.

[13] Digikey. "BC1910-ND: 330 NF Film Capacitor, 1 KV, Radial." Web. 18 Apr. 2013. <http://www.digikey.com/product-search/en?vendor=0&keywords=bc1910-nd>.

[14] Digikey. "HS276-ND: TO-220 Heat Sink." Web. 22 Apr. 2013. <http://www.digikey.com/product-search/en?WT.z_header=search_go&lang=en&site=us&keywords=hs276-nd&formaction=on&x=0&y=0>.

[15] Engineer's Handbook. "Engineering Materials - Non Ferrous Metals." Web. 29 Jan. 2014. <http://www.engineershandbook.com/Materials/nonferrous.htm>.

[16] Engineering Toolbox. "Air - Absolute and Kinematic Viscosity." Web. 23 Feb. 2014. <http://www.engineeringtoolbox.com/air-absolute-kinematic-viscosity-d_601.html>.

[17] Engineering Toolbox. "Air - Density and Specific Weight." Web. 23 Feb. 2014. <http://www.engineeringtoolbox.com/air-density-specific-weight-d_600.html>.

[18] Engineering Toolbox. "Air Properties." Web. 23 Feb. 2014. <http://www.engineeringtoolbox.com/air-properties-d_156.html>.

[19] Engineering Toolbox. "Metals - Melting Temperature." Web. 28 Jan. 2014. <http://www.engineeringtoolbox.com/melting-temperature-metals-d_860.html>.

[20] Engineering Toolbox. "Thermal Conductivity of Some Common Materials and Gases." Web. 23 Feb. 2014. <http://www.engineeringtoolbox.com/thermal-conductivity-d_429.html>.

[21] Esselman, W. H. "The NERVA Nuclear Rocket Reactor Program." *Westinghouse Engineer* 25.3 (1965): 65-75. Print. <http://pbhistoryb1b3.grc.nasa.gov/assets/history/B%20NERVA/NERVA%20Nuclear%20Rocket%20Program%20(1965).PDF>.

[22] Fairchild Semiconductor. *Induction Heating System Topology Review*. Tech. no. AN-9012.: Fairchild Semiconductor, 2000. Print.

[23] Fortuner 4x4. "Wire Gauge Calculation Chart - Maximum Current Draw." *Fortuner 4x4 Fans*. Web. 15 Apr. 2013. <http://www.fortuner4x4fans.co.za/forum/index.php?page=Attachment&attachmentID=299&h=be8b440dbf9c008d2615285ebd0599ef25ddea6d>.

[24] Future Electronics. "Schottky Rectifiers." Web. 20 Apr. 2013. <http://www.futureelectronics.com/en/diodes/schottky-rectifiers.aspx>.

[25] General Applied Science Laboratory (GASL) (1995). *Systems Operation Manual for Pebble Bed Hydrogen Heater installed at NASA John C. Stennis Space Center.* Ronkonkoma, NY. Print.

[26] GH Induction Atmospheres. "Innovative Induction Heating." Web. 2 July 2013. <http://www.gh-ia.com/induction_heating.html>.

[27] Grainger. "1WLH5: Flange, Cast Copper, C x Flange, 1 in." Web. 2 Apr. 2013. <http://www.grainger.com/product/NIBCO-Flange-1WLH5?s_pp=false>.

[28] Hobby Lobby. "491621: Large Activ-Wire Mesh, Aluminum." Web. 9 Apr. 2013. <http://shop.hobbylobby.com/products/large-activ-wire-mesh-491621/>.

[29] Home Depot. "123100: Homax Fine Bronze Wool Pads (3 Pack)." Web. 6 Apr. 2013. <http://www.homedepot.com/p/Homax-Fine-Bronze-Wool-Pads-3-Pack-123100/100185012>.

[30] Houts, M. G., et al. "Nuclear Thermal Propulsion for Advanced Space Exploration." NASA (2011). *NTRS*. Print. <http://ntrs.nasa.gov/archive/nasa/casi.ntrs.nasa.gov/20120014974_2012014786.pdf>.

[31] Iatcheva, Ilona, Georgi Gigov, Georgi Kunov, and Rumena Stancheva. "Analysis of Induction Heating System for High Frequency Welding." *Electrical Engineering* 25.3 (2012): 183-91. Print.

[32] Jackson, John D. *Classical Electrodynamics*. 3rd ed.: Hamilton Printing, 1999. Print.

[33] Kreith, Frank, and Mark S. Bohn. *Principles of Heat Transfer*. 6th ed. Ontario: Chris Carson, 2001. Print.

[34] Lancashire, R. B., E. A. Lezberg, and J. F. Morris. "Heat-Transfer Coefficients for Full-Scale Pebble-Bed Heater." *Industrial and Engineering Chemistry* 52.5 (1960): 433-34. Print.

[35] Lupi, S. "The Calculation of Planar Circular Coils for the Induction Heating of Bimetallic Plates." *Archiv Fur Elektrotechnik* 60.6 (1978): 313-318. *Springer*. Web. 27 Jan. 2014.

[36] Materkowski, Dave. "How NASA's NERVA Rocket Engine Works." *ART 101*. Web. 20 Jan. 2014. <http://www.personal.psu.edu/djm5200/NERVA.html>.

[37] McCurrie, R. A. *Ferromagnetic Materials: Structure and Properties*. San Diego: Academic, 1994. Print.

[38] Meng, L.; Cheng, K.; Chan, K. “Heating Performance Improvement and Field Study of the Induction Cooker.” *Power Electronics Systems and Applications, 2009. PESA 2009. 3rd International Conference* (May 2009): 1-5. Presented.

[39] Mouser. "70-IHV-15-500: 500 uH Inductor, Radial." Web. 17 Apr. 2013. <http://www.mouser.com/ProductDetail/Vishay/IHV15BZ500/?qs=%2fha2pyFadugmQTbFDrnuErOv8Ng0ztPFw8%2fYvy%2fHTBqda9UGY3u0dA%3d%3d>.

[40] MSC Industrial Supply. "00073239: Carbon Steel Ball Bearing, 1/8 Inch." Web. 7 Apr. 2013. <http://www.mscdirect.com/product/00073239?rItem=00073239>.

[41] Mühlbauer, Alfred. "Background of Induction Heating." *History of Induction Heating and Melting*: Vulkan-Verlag GmbH, 2008. Print.

[42] NASA. "Aerial A,B." *Stennis Image Retrieval System*. 30 Apr. 2004. Web. 20 Jan. 2014. <http://www.ssc.nasa.gov/sirs/scripts/getxmlfile.pl?id=SSC-2004-02813>.

[43] NASA. Glenn Research Center. *The NASA Glenn Research Center's Hypersonic Tunnel Facility*. By Mark R. Woike and Brian P. Willis. 2001. Print.

[44] NASA. Lewis Research Center. *An Historical Perspective of the NERVA Rocket Engine Technology Program*. By W. H. Robbins and H. B. Finger. 1991. Print.

[45] NASA. "NERVA Engine Testing." *History B-1 and B-3 Test Stands*. NASA. Web. 27 Jan. 2014. <http://pbhistoryb1b3.grc.nasa.gov/NERVA.aspx>.

[46] NASA. "Static Test Firing of Saturn V S-1C Stage." *Great Images in NASA*. 1 Jan. 1967. Web. 20 Jan. 2014. <http://dayton.hq.nasa.gov/IMAGES/LARGE/GPN-2000-000041.jpg>.

[47] NDT Resource Center. "The Hysteresis Loop and Magnetic Properties." Web. 7 July 2013. <http://www.ndt-ed.org/EducationResources/CommunityCollege/MagParticle/Physics/HysteresisLoop.htm>.

[48] Norton, O. & Palmer, R. (2005). *Technology to Support the Design of a Nuclear Propulsion and Power Test Facility.* DIAL at Mississippi State University. Stennis Space Center, MS. Print.

[49] Omega. "PX157-005DI Manual: Differential Pressure Transducer." Web. 11 Apr. 2013. <http://www.omega.com/Manuals/manualpdf/M1997.pdf>.

[50] Omega. "Thermocouples." Web. 10 Apr. 2013. <http://www.omega.com/prodinfo/thermocouples.html>.

[51] Omega. "TMQSS-062G-6: T-Type, 6 Inch, Grounded, 1/16 Inch." Web. 10 Apr. 2013. <http://www.omega.com/pptst/JMQSS.html>.

[52] Omega. "Type T Revised Thermocouple Reference Tables." Web. 10 Apr. 2013. <http://www.omega.com/temperature/Z/pdf/z223.pdf>.

[53] Osborn, H. B., Jr., et al. *Induction Heating*. Cleveland: 1946. Print.

[54] Osofsky, Irving B. Pebble-Bed Heater and Shock Tube Assembly. Sparta, Inc., assignee. Patent US 5197323 A. 13 July 1990. Print.

[55] Palaszewski, B. (2004). *Nuclear and Future Flight Propulsion: Vehicle Design Case Studies*. Glenn Research Center. Cleveland, OH. Print.

[56] Plumbing Supply. "Rigid Copper Pipe." Web. 1 Apr. 2013. <http://www.plumbingsupply.com/copperpipe.html>.

[57] Pryor, Larry, Rick Schlobohm, and Bill Brownell. "A Comparison of Aluminum vs. Copper as Used in Electrical Equipment." GE Consumer and Industrial. Web. 11 Feb. 2014. <http://apps.geindustrial.com/publibrary/checkout/Alum-Copper?TNR=White%20Papers%7CAlum-Copper%7Cgeneric>.

[58] Rauch, R.; Coote, D.; Junnell, J.; & Ryan, H. (2011). *The Nuclear Propulsion and Power Non-Nuclear Test Facility CIF Request*. Stennis Space Center. Print.

[59] Rauch, R. & Raines, N. *Technology to Support the Design of a Nuclear Propulsion and Power Non-nuclear Test Facility CDDF Final Report.* (2005). Stennis Space Center. Print.

[60] Rhoades, Nathan. "A Fundamental Overview of Heating by Induction." (2006). Web. 26 Jan. 2014. Print.

[61] RMCybernetics. "A DIY Induction Heater." *Research Media and Cybernetics*. Web. 20 Apr. 2013. <http://www.rmcybernetics.com/projects/DIY_Devices/diy-induction-heater.htm>.

[62] RMCybernetics. "RES0W6: 240 Ohm Resistor, 0.6 Watt." Web. 19 Apr. 2013. <http://www.rmcybernetics.com/shop/electronic-components/resistors/resistors-0.6W>.

[63] Russo, E.; Rieder, P.; Castrogiovanni, A.; St. Cyr, W. (1996). *Thermal Analysis of NASA's John C. Stennis Space Center's Pebble-Bed Heater*. Stennis Space Center. Stennis Space Center, MS. Print.

[64] Serway, Raymond A., and John W. Jewett, Jr. *Physics for Scientists and Engineers with Modern Physics*. 7th ed. Belmont, CA: Thomson/Brooks/Cole, 2008. Print.

[65] Simons, E.N. *A Dictionary of Alloys*. Cornell University. 1970. Print.

[66] ST Microelectronics. *STP30NF10 MOSFET Manual*. Web. 25 Apr. 2013. <http://www.st.com/web/en/resource/technical/document/datasheet/CD00002440.pdf>.

[67] Stansel, N. R. *Induction Heating*. 1st ed. New York City: McGraw-Hill Book, 1949. Print.

[68] Stratasys. "ABS." Web. 31 Jan. 2014. <http://www.nrri.umn.edu/NLTC/ABS07.pdf>.

[69] Swagelok. "B-1RS4: Brass, Needle Valve, 1/4 In, T-shape." Web. 4 Apr. 2013. <http://www.swagelok.com/search/find_products_home.aspx?part=B-1RS4&item=>.

[70] Swagelok. "B-42S4: Brass, Ball Valve, 1/4 In, T-shape." Web. 31 Jan. 2014. <http://www.swagelok.com/search/find_products_home.aspx?part=B-42S4&item=5c7e79e8-62ca-4c16-8b6e-0ba1530cbfd7>.

[71] Swagelok. "B-100-1-2BT: Brass, Straight Tube Fitting, 1/16 In, Male NPT, Bored-Through." Web. 11 Apr. 2013. <http://www.swagelok.com/search/find_products_home.aspx?part=B-100-1-2BT&item=>.

[72] Swagelok. "B-400-1-4: Brass, Straight Tube Fitting, 1/4 In, Male NPT." Web. 4 Apr. 2013. <http://www.swagelok.com/search/find_products_home.aspx?part=B-400-1-4&item=20b6dcb5-5a04-42f1-9df7-a5d3fd3672c3>.

[73] Swagelok. "B-400-1-4BT: Brass, Straight Tube Fitting, 1/4 In, Male NPT, Bored-Through." Web. 11 Apr. 2013. <http://www.swagelok.com/search/find_products_home.aspx?part=B-400-1-4BT&item=>.

[74] Tech Power Up. "What Is a MOSFET, What Does It Look Like, and How Does It Work?" 24 May 2004. Web. 6 Feb. 2014. <http://www.techpowerup.com/articles/overclocking/voltmods/21>.

[75] Tudbury, C. A. "Electromagnetics in Induction Heating." *IEEE Transactions on Magnetics* 10.3 (1974): 694-97. *IEEE*. Web. 25 Jan. 2014. Print.

[76] Weber, Louis J. Pebble Heater System and Method of Operation. Phillips Petroleum Company, assignee. Patent US 2,530,274. 9 Dec. 1946. Print.

[77] Wtshymanski. "Induction Cooktop Rolling Boil." CommonsHelper, 6 Jan. 2011. Web. 27 Jan. 2014.

[78] Yoder, Graydon L., et al. *An Experiment to Study Pebble Bed Liquid-Fluoride-Salt Heat Transfer*. Proc. of ICAPP, Nice, France. 2013. Print.

[79] Youhua, Wang, Wang Junhua, Li Jiangui, and Li Haohua. "Analysis of Induction Heating Eddy Current Distribution Based on 3D FEM." *Computational Technologies in Electrical and Electronics Engineering* (2008): 238-41. *IEEE Xplore*. Web. 20 Mar. 2013.

[80] 80/20 Inc. "80/20 Home Page." Web. 3 Feb. 2014. <http://www.8020.net/Default.asp>.

APPENDIX

1) Step-by-step assembly process of the pebble-bed heater:

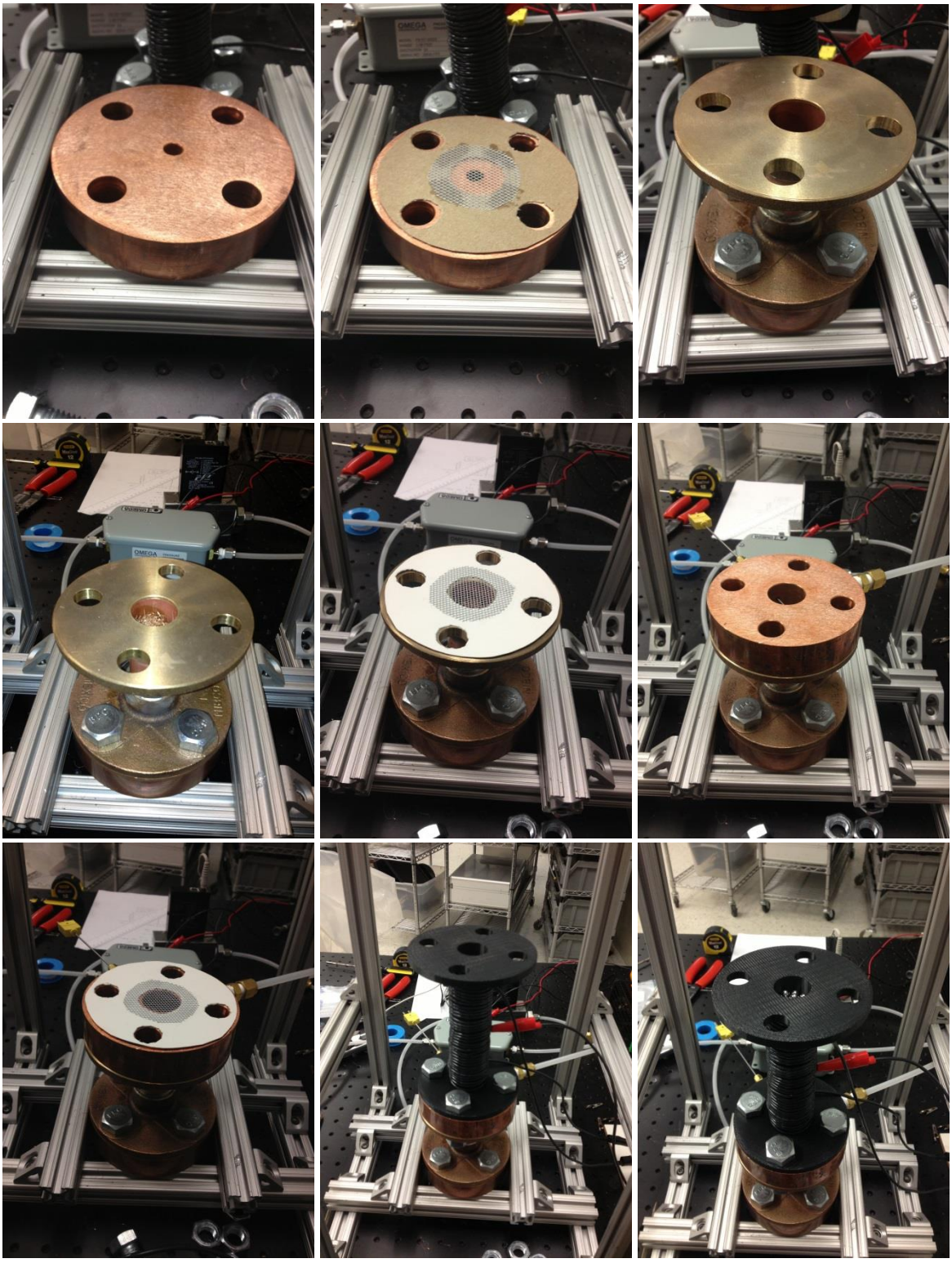

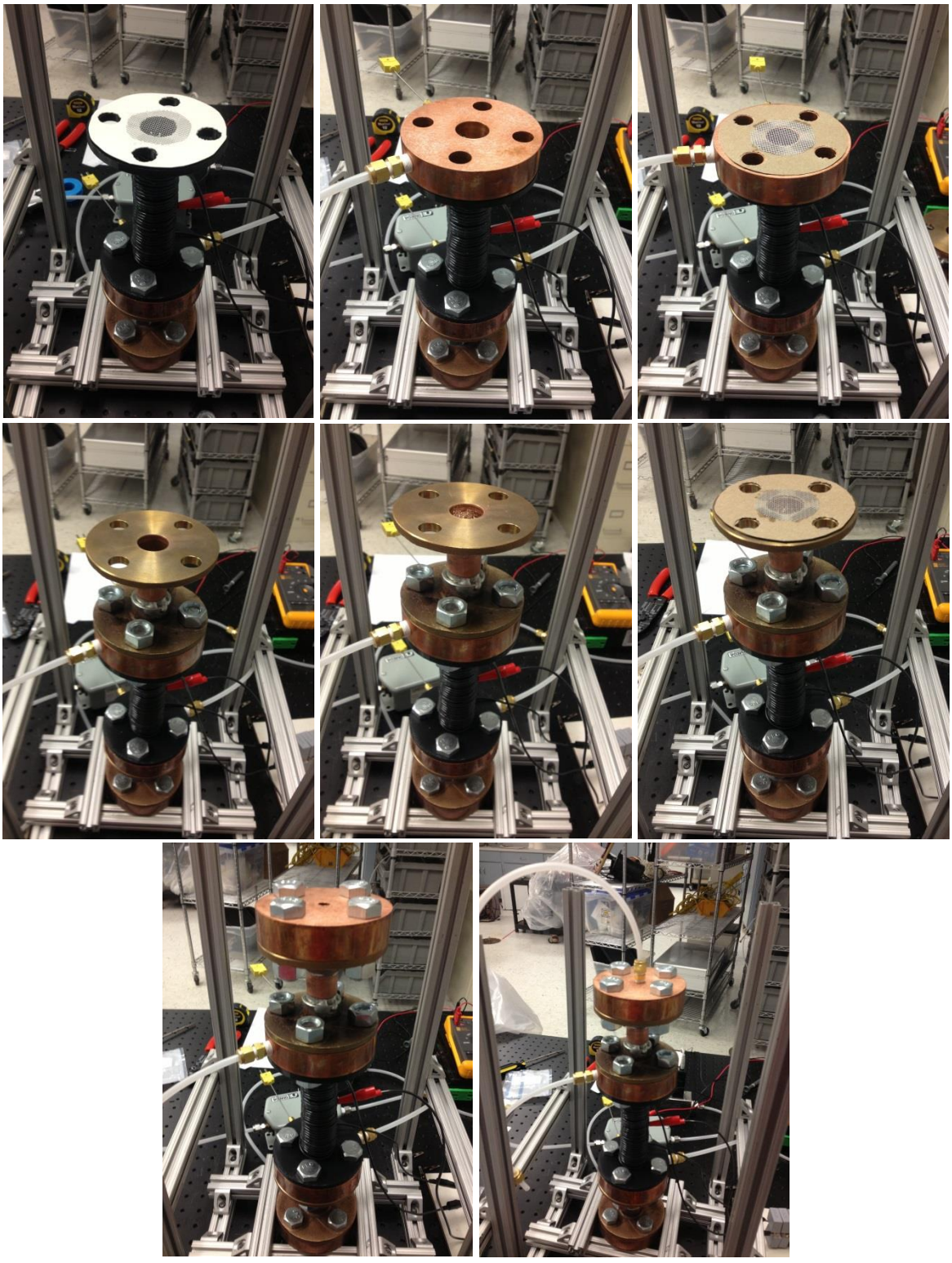

2) Extra Uncertainty Data:

U_Current	0.05	A	
U_Voltage	0.005	V	
U_vol_flow	8.3333E-06	m3/s	
U_Density	0	kg/s	
U_Temp	0.1111111	K	
U_c_p	0	J/kg-K	
U_k_plastic	0	W/m-K	
U_L_wall	0	m	
U_r_out	0	m	
U_r_in	0	m	
U_number	0	--	
U_r_ball	0	m	
U_freq	10	Hz	
r_in	0.0127	m	(0.5")
r_out	0.01905	m	(0.75")
L_wall	0.1397	m	(5.5")
k_plastic	0.25	W/m-K	

U_massflow	U_ΔT	U_Q_conv	U_ΔT_wall	U_Q_loss	U_Q_cond	U_N_HT	U_Np	U_Nu/Np
[kg/s]	[K]	[W]	[K]	[W]	[W]	[--]	[--]	[--]
8.525E-06	0.157	0.418	0.1571	0.085	0.418	0.053	1.88E-12	2.368
9.242E-06	0.157	0.247	0.1571	0.085	0.247	0.061	1.41E-12	3.034
9.500E-06	0.157	0.123	0.1571	0.085	0.123	0.071	9.36E-13	4.054
8.250E-06	0.157	0.491	0.1571	0.085	0.491	0.043	1.88E-12	1.914
8.792E-06	0.157	0.304	0.1571	0.085	0.304	0.047	1.41E-12	2.334
9.392E-06	0.157	0.142	0.1571	0.085	0.142	0.054	9.36E-13	3.075
7.983E-06	0.157	0.576	0.1571	0.085	0.576	0.035	1.88E-12	1.576
8.708E-06	0.157	0.365	0.1571	0.085	0.365	0.039	1.41E-12	1.946
9.367E-06	0.157	0.170	0.1571	0.085	0.170	0.044	9.36E-13	2.480
8.458E-06	0.157	0.442	0.1571	0.085	0.442	0.052	1.88E-12	2.281
9.183E-06	0.157	0.271	0.1571	0.085	0.271	0.061	1.41E-12	2.923
9.542E-06	0.157	0.141	0.1571	0.085	0.141	0.070	9.36E-13	3.862
8.167E-06	0.157	0.534	0.1571	0.085	0.534	0.042	1.88E-12	1.842
8.833E-06	0.157	0.335	0.1571	0.085	0.335	0.048	1.41E-12	2.295
9.358E-06	0.157	0.182	0.1571	0.085	0.182	0.053	9.36E-13	2.932
7.884E-06	0.157	0.613	0.1571	0.085	0.613	0.035	1.88E-12	1.515
8.542E-06	0.157	0.407	0.1571	0.085	0.407	0.039	1.41E-12	1.854
9.833E-06	0.157	0.222	0.1571	0.085	0.222	0.047	9.36E-13	2.579
8.167E-06	0.157	0.530	0.1571	0.085	0.530	0.051	1.88E-12	2.192
8.833E-06	0.157	0.338	0.1571	0.085	0.338	0.059	1.41E-12	2.776
9.333E-06	0.157	0.191	0.1571	0.085	0.191	0.066	9.37E-13	3.608
7.884E-06	0.157	0.615	0.1571	0.085	0.615	0.042	1.88E-12	1.774
8.575E-06	0.157	0.410	0.1571	0.085	0.410	0.047	1.41E-12	2.223
9.583E-06	0.157	0.245	0.1571	0.085	0.245	0.056	9.37E-13	3.056
7.689E-06	0.157	0.691	0.1571	0.085	0.691	0.035	1.88E-12	1.486
8.330E-06	0.157	0.484	0.1571	0.085	0.484	0.038	1.41E-12	1.813
9.042E-06	0.157	0.304	0.1571	0.085	0.304	0.043	9.37E-13	2.327